X-734-68-460
PREPRINT

RESEARCH AND DEVELOPMENT IN NEEDLE AND SLIT COLLOID THRUSTERS

KENNETH W. STARK
ALLAN SHERMAN

NOVEMBER 1968

GSFC
GODDARD SPACE FLIGHT CENTER
GREENBELT, MARYLAND

X-734-68-460

RESEARCH AND DEVELOPMENT IN NEEDLE AND SLIT COLLOID THRUSTERS

Kenneth W. Stark

and

Allan Sherman

Auxiliary Propulsion Branch

November 1968

GODDARD SPACE FLIGHT CENTER

Greenbelt, Maryland

RESEARCH AND DEVELOPMENT IN NEEDLE AND SLIT COLLOID THRUSTERS

Kenneth W. Stark and Allan Sherman

ABSTRACT

A thorough familiarization and test program was conducted in capillary needle colloid thruster technology. This technology is basically a means by which electrostatic particle spraying can be achieved through the use of slightly conductive propellants and high voltages.

Forty-eight single needle tests were run with various needle materials and geometries using several propellant combinations. Several test facility variations were employed to study secondary electron effects.

During this time two slit sources were designed and built. After the single needle testing was terminated the annular slit thruster was tested successfully.

Future efforts will concentrate on continued testing of the annular slit thruster to perfect its overall performance.

TABLE OF CONTENTS

RESEARCH AND DEVELOPMENT IN NEEDLE AND SLIT COLLOID THRUSTERS

INTRODUCTION

For approximately eight years, research and development has been conducted in the field of electrostatic charged particle (colloid) propulsion. Briefly, colloid thrusters operate by the electrostatic spraying of liquids. The propellant, a low vapor pressure moderately conductive liquid, is sprayed from the rims of metallic capillary needles or slits which are maintained at high electric potential. This potential imparts a force on the liquid interface causing the expulsion of very small charged particles. The very low power required for this charged particle formation is the feature which makes colloid thrusters competitive with ion engines, especially at thrust levels below one millipound.

Since the early reports on single needle colloid thruster tests[4,8] colloid needle-type thruster research and development has shown significant advancement. Multiple needle module test runs,[1] on the order of 1000 consecutive hours at 800 seconds specific impulse, and a 50 hour duration test on a 73 needle bipolar array[5] have been reported.

With this initial emphasis in needle type thrusters, relatively little has been accomplished in the development of single units of one flow area capable of producing high thrusts. It therefore was the ultimate purpose of this program to conduct research and development in this area resulting in single high thrust units which, in their inherent simplicity, would offer obvious advantages over multiple needle arrays.

Preliminary to this, a series of single needle tests were run in order to gain familiarization with colloid thruster operation and testing techniques and to gain knowledge which could be used in designing the advanced geometry. In addition, along with this needle testing, an analytical study[7] of the colloid dispersion process was conducted. This report describes the overall test procedure, apparatus utilized, needle testing results, a summary of the data reduction program employed and a complete presentation of the design and testing of the new single high thrust unit (annular slit).

DATA REDUCTION

Before proceeding with the discussion of the results of this program it is appropriate to describe the method by which performance of these thrusters is evaluated. Ideally, the optimum procedure for testing and evaluating thruster

performance would be to utilize a direct thrust measurement system and an absolute flow measuring device. Unfortunately, at this time, suitable means for directly measuring thrust and flow rates for these experimental laboratory models are not available.

Present methods of reducing data utilizes a technique developed early in the history of colloid thruster technology.[3,4] Basically, this method employs the time of flight (TOF) trace which is numerically integrated to yield thrust, specific impulse, charge to mass ratios, efficiency, mass flow rates and average particle velocity.

A TOF trace is obtained by simultaneously grounding the needle voltage and recording the current decay curve caused by the particles in flight after grounding. A typical TOF curve is shown in Figure 1.

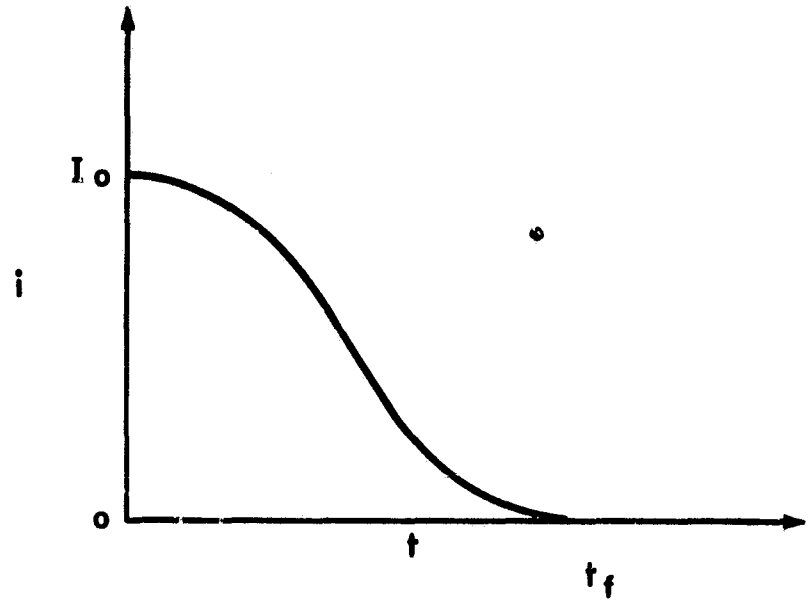

Figure 1. Typical time of flight trace.

A computer program was written for the reduction of data obtained from the TOF curves which computes the colloid thruster performance parameters from inputs of sets of points of current and time. These points are obtained from enlarged photographs (8" × 10") of the original oscilloscope picture (3" × 5").

The sets of points are used in the program to numerically evaluate the following two integrals which are required for the TOF equations:

$$X_1 = \int_0^{t_f} i\,dt \qquad (1)$$

$$X_2 = \int_0^{t_f} it\, dt . \qquad (2)$$

The numerical method selected for the evaluation of these integrals is Simpson's 1/3 rule. Hence,

$$X_1 = \frac{\Delta t}{3}\left[i_0 + 4i_1 + 2i_2 + 4i_3 + 2i_4 + \cdots 4i_{N-1} + i_N \right] + \text{error term} \qquad (3)$$

and

$$X_2 = \frac{\Delta t}{3}\left[i_0 t_0 + 4i_1 t_1 + 2i_2 t_2 + 4i_3 t_3 + 2i_4 t_4 + \cdots 4i_{N-1} t_{N-1} + i_N t_N \right] + \text{error term} \qquad (4)$$

where N should be an even number.

The error involved in the above calculations was evaluated in the following way. First, the integral for a typical TOF trace was evaluated by the above equations with both 11 and 19 sets of points. Second, the same calculation was made using the generally less accurate Trapezoid rule to numerically evaluate these integrals. The results of these calculations for X_1 are summarized in the following table:

	11 points	19 points	% Diff.
Simpson	14.827	14.827	0
Trap.	14.880	14.840	.27
% Diff.	.36	.086	

In both of the above cases the negligible change in the value of X_1 in increasing N from 11 to 19 shows that the error terms in Equations (3) and (4) are extremely small for $N \geq 11$. Similarly, the close agreement between the results obtained by the Trapezoid and Simpson's Rule show that the error in using either method for $N \geq 11$ is negligible. Since similar results were also

obtained for the computation of X_2, for the data reported herein the minimum number of point sets was 13, it can be concluded that X_1 and X_2 are computed to a high degree of accuracy by the data reduction program.

Once X_1 and X_2 are calculated the program then computes the test performance parameters by the standard TOF equations.

$$T = \frac{2V}{d} X_1 \tag{5}$$

$$m = \frac{4V}{d^2} X_2 \tag{6}$$

$$ACMR = \frac{I_c}{m} \tag{7}$$

$$\eta = \frac{T^2}{2VI_c\, m} \tag{8}$$

$$\eta_b = \frac{q/m}{ACMR} \tag{9}$$

$$I_{sp} = \frac{T}{mg_0} \tag{10}$$

LABORATORY APPARATUS AND PROCEDURE

To conduct testing of the colloid thrusters it is necessary to operate them in a vacuum environment as the voltage necessary to operate the various configurations could range from 6 KV to 25 KV. With these high voltages and thin rimmed firing edges it is very easy to produce corona discharges. Also the high velocity particles would have air drag acting on them thus producing erroneous TOF results.

Figure 2 shows the basic vacuum chamber setup utilized whereby the needles and collector are in a horizontal firing position. When the annular slit testing began it was necessary to assume the vertical position in order to minimize the effect of gravity on the meniscus and beam trajectory. However, for both the vertical and horizontal arrangements, the test procedure and operation is the same and is as follows.

After each propellant combination is mixed and before each run the propellant is degassed under vacuum. This is to assure that air and other

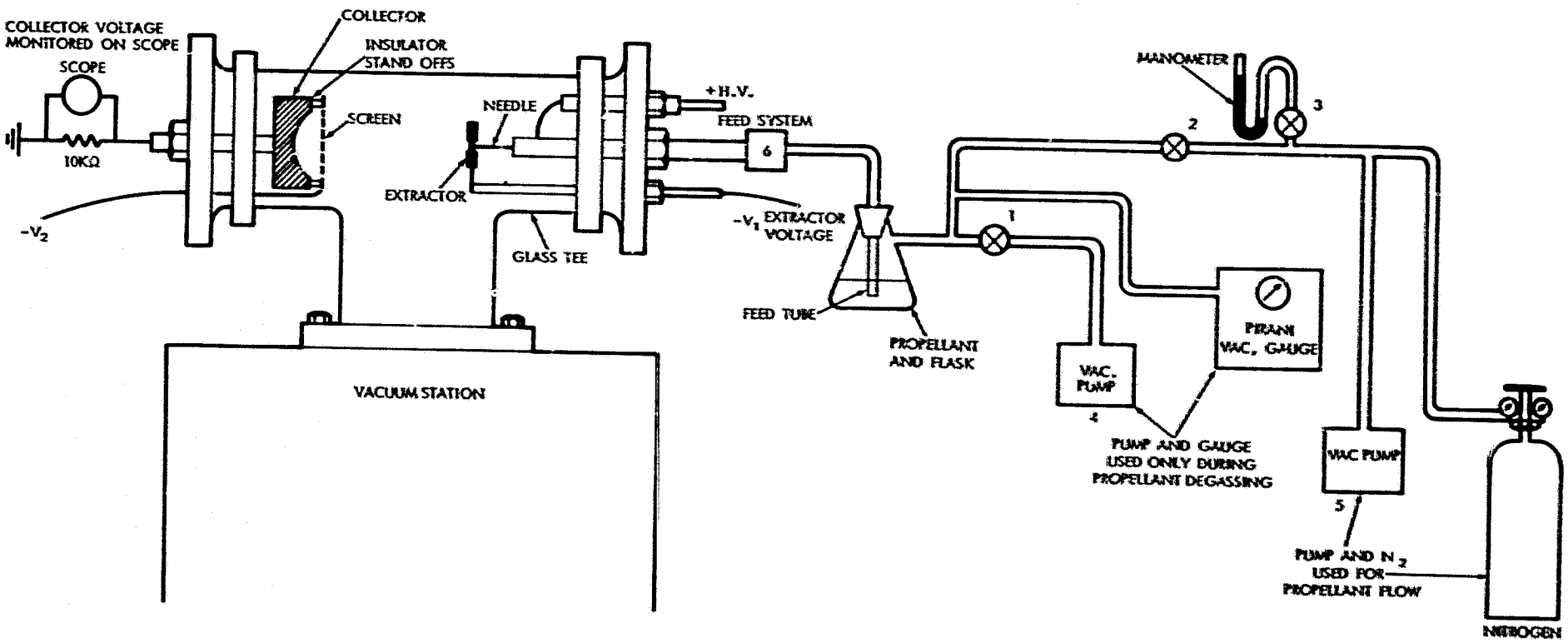

Figure 2. Vacuum chamber test setup.

higher vapor pressure contaminants (e.g. water) are removed. If this is not done erratic performance and corona will result during operation. For this procedure the propellant feed tube is raised above the level of propellant and clamped at point 6 (Figure 2). The propellant is heated and stirred while the vacuum pump (4) is operating. The Pirani vacuum gauge is used to monitor the pressure. During this procedure valve 1 is open and valve 2 is closed. After degassing is completed the propellant is cooled to room temperature, the clamp (6) is removed, the feed tube is inserted into the propellant, valve (1) is closed and the vacuum pump (4) is shut off. To initiate propellant flow the vacuum pump (5) is turned on, valves (2) and (3) are opened and the nitrogen gas supply is turned on until the correct pressure differential is observed on the manometer.

When the propellant reaches the firing surface of the needles or slits the high voltage is applied to the thruster. Negative voltages are applied to the extractor and screen. The charged particles expelled from the thruster impinge upon the collector resulting in a current which flows through a resistor to ground. The voltage across this resistor is monitored on an oscilloscope and from this the diagnostic test procedures are conducted as described in a previous section. Figures 3 and 4 show schematic representations of the thruster voltage

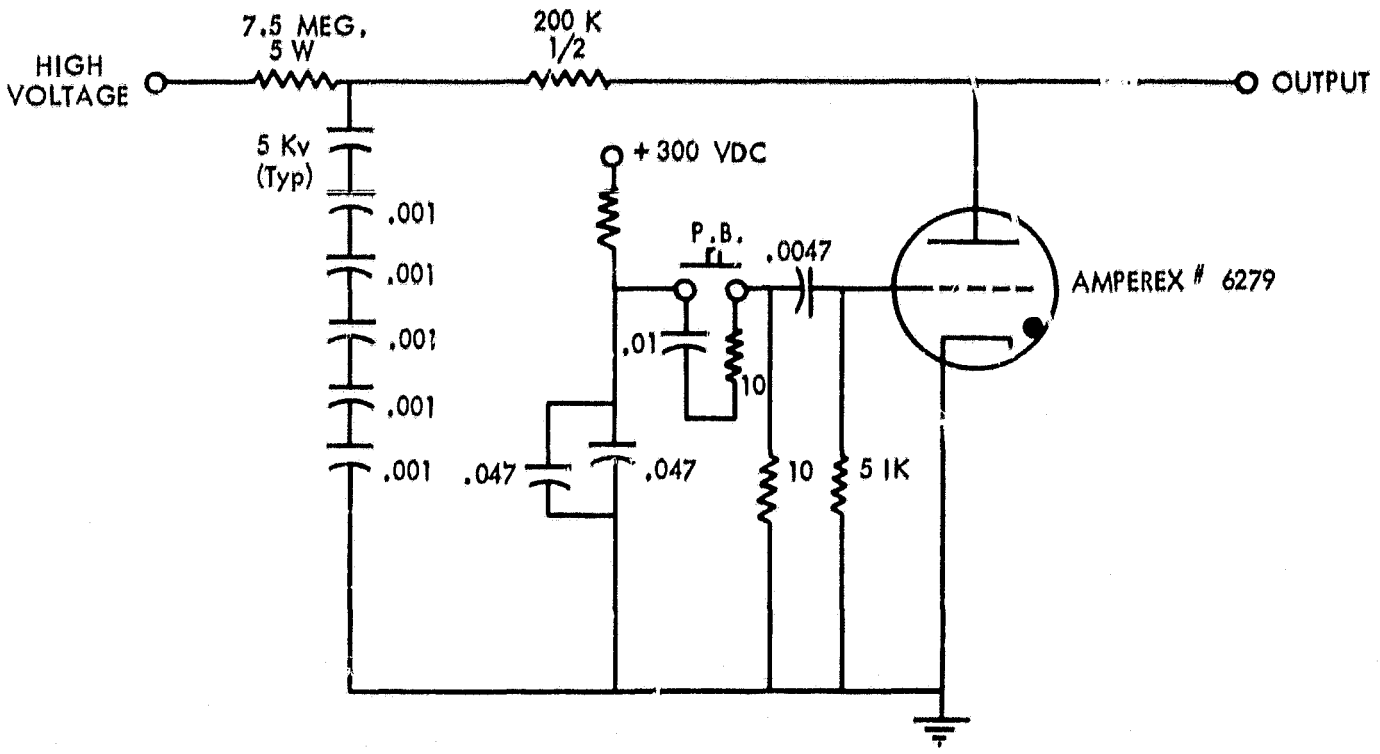

Figure 3. Thyratron zapper circuit.

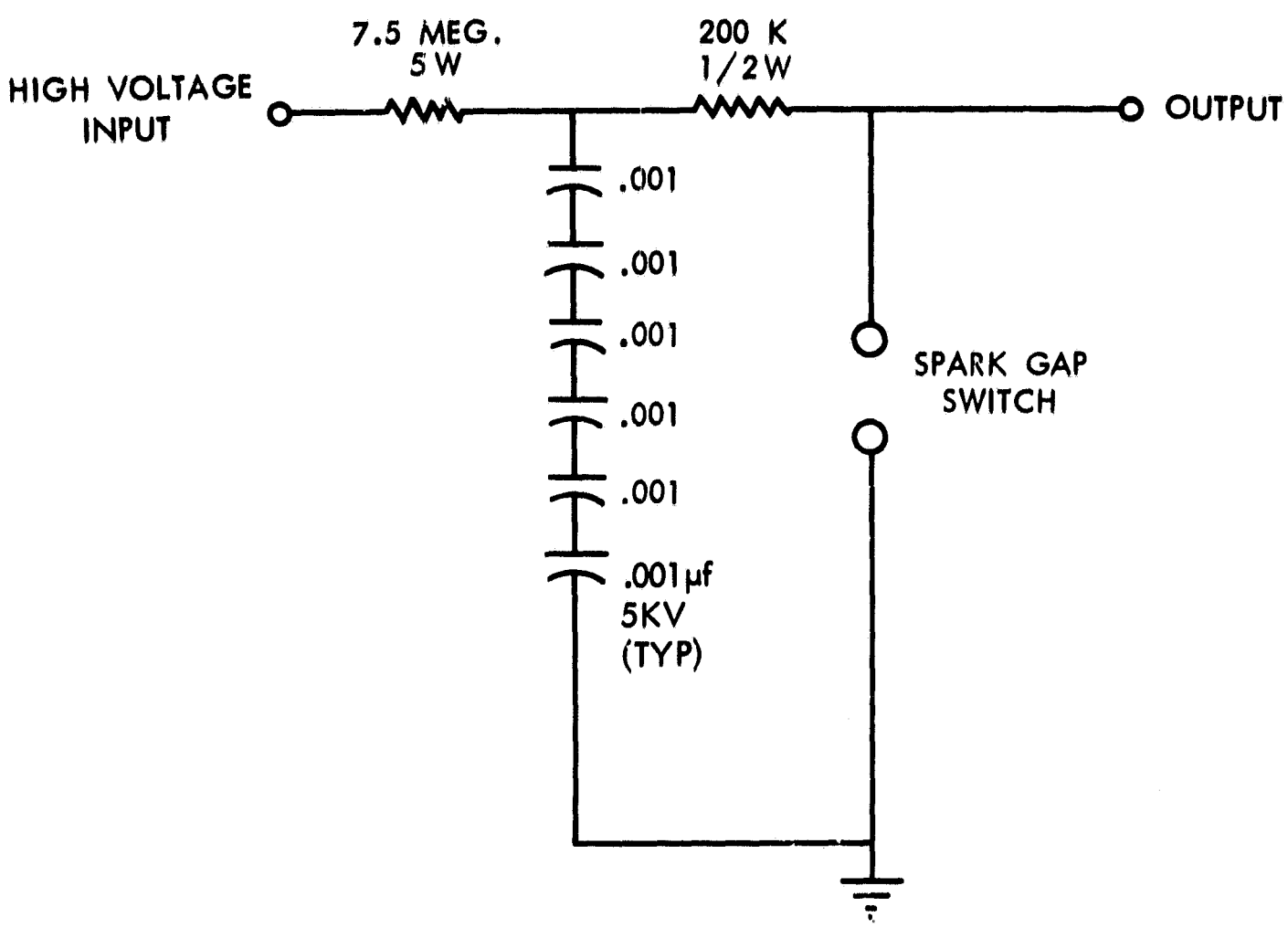

Figure 4. Ball zapper circuit.

shorting (zapper) units used to obtain the TOF traces. As mentioned previously these units accomplish the dual purpose of simultaneously grounding the thruster voltage and triggering the scope to register the current of all particles in flight at the moment of the grounding.

CAPILLARY NEEDLE TEST PROGRAM

Prior to the main pursuit of the colloid thruster program, that of developing a high thrust high performance slit thruster, it was necessary to conduct a familiarization program centered around the already existing capillary needle technology.

Forty-eight needle tests were run in this program. Included in these tests, in addition to the familiarization process, were investigations into performance of different propellants, determining effect on performance of variations in

extractor size and potential, effect of shield and screen voltages on secondary electron emission, performance of different needle tip geometries and determining the best needle material for minimizing tip errosion due to the effect of high voltage combined with the low vacuum and electrolytic type propellants.

A summary of the significant needle testing results is presented in Table 1.

A. Factors Influencing Secondary Electron Emission and Performance

One of the most difficult problems to evaluate in colloid testing is that of secondary emission. For example, secondary electron emission can occur at the collector, suppressor screen, end plates of the vacuum chamber, or at the needle assembly. In fact, because of the high energy of the colloid particles (on the order of 10^7 times the work function of most metals), it is conceivable to have either the original colloid droplet or shattered fragments of the original droplet initiate secondary electron emission at any metallic surface within the chamber. In addition, it is suggested by the authors of Reference 1 that these particles which result from shattering upon impact with the collector might maintain a positive charge. Thus "positive secondaries" may also be produced in the chamber.

There are many possible disturbances upon performance that can be generated by secondary electrons. Three of the most prominent effects experienced in this test program will be discussed.

The first and most difficult to interpret is the positive overshoot experienced on the TOF trace as shown in Figure 5. The difficulty arises here in the reduction of the TOF trace to obtain performance data.

The positive overshoot of the TOF trace may be explained in terms of secondary emission effects. For example, assume that at steady state conditions the spray into the collector contains a substantial number of secondary electrons as well as the positively charged propellant droplets. Now, after the zap the rate of secondary electron emission decreases as the higher velocity particles reach the collector. At the same time the electrons in the beam, which are of higher velocity than the positive particles, are being reabsorbed either at the collector or elsewhere in the chamber. Hence, there is a net rate of decrease of electrons in the beam. If this rate of decrease of negative charge is larger than the rate of decrease of positive charge that reaches the collector, an initial positive overshoot would occur. After a very short time, however, the secondary electron effect becomes negligible and the TOF assumes its usual shape.

It should be noted that for the tests reported herein in which a positive overshoot occurred, the current was taken at the steady state value for the duration of the overshoot. This produces an error in the results. However, since TOF

FOLDOUT FRAME /

Table 1

Summary of Single Needle Tests

Test #	Purpose of Test	Needle	Propellent	P_f (MM Hg)	V_N (Volts)	V_{EXT} (Volts)	V_{SCR} (Volts)	I_C (μA)	I_N (μA)	I_{EXT} (μA)	$\left(\frac{\text{ACMR Coul.}}{\text{Kg}}\right)$
13P	General Testing of Hastelloy C Needle	Hastelloy C	NaI (20g)/ Glyc. (100 Ml)	160	6000	– 500	–45	.79			2641
14P	General Testing of Hastelloy C Needle	Hastelloy C	NaI (20g)/ Glyc. (100 Ml)	160	6000	– 500	–45	.62			2917
15P	General Testing of Hastelloy C Needle	Hastelloy C	NaI (20g)/ Glyc. (100 Ml)	160	6000	– 500	–45	.68			4163
16P	General Testing of Hastelloy C Needle	Hastelloy C	NaI (20g)/ Glyc. (100 Ml)	160	6000	– 500	–45	.55			3698
17P	General Testing of Hastelloy C Needle	Hastelloy C	NaI (20g)/ Glyc. (100 Ml)	160	6000	– 500	–45	.73			3998
18P	General Testing of Hastelloy C Needle	Hastelloy C	NaI (20g)/ Glyc. (100 Ml)	160	6000	– 500	–45	1.0			3652
19P	General Testing of Hastelloy C Needle	Hastelloy C	NaI (20g)/ Glyc. (100 Ml)	160	6000	– 500	–45	.82			3074
20P	To determine the effect of screen voltage on steady state values and TOF results.	Hastelloy C	NaI (20g)/ Glyc. (100 Ml)								
1.				153	5900	– 473	–22	.87	2.2	1.89×10^{-2}	1329
2.				153	5900	– 473	–45	.63	1.62	1.89×10^{-2}	1004
3.				153	5900	– 473	–67	.55	1.99	1.25×10^{-2}	1092
4.				153	5900	– 473	–90	.53	1.90	2.5×10^{-2}	924.8
5.				153	5900	– 473	Ground	1.27	2.8	2.65×10^{-2}	1476
6.				153	5900	– 473	–45	.70	2.45	2.25×10^{-2}	996.3
21P	To determine the effect of screen stand-off distance on steady state values and TOF results.	Platinum	NaI (20g)/ Glyc. (100 Ml)								
1.				110	7100	– 473	Ground	2.14	6	.55	2240
2.				110	7100	– 473	–45	.70	5.8	.52	1677
3.				110	7100	– 473	–67	.67	5.65	.45	1693
4.				110	7100	– 473	–90	.65	5.9	.51	1935
5.				110	7100	– 473	–22	.79	5.65	.45	1739
22P	Rerun of 21P but with glass feed system.	Platinum	NaI (20g)/ Glyc. (100 Ml)								
1.				112	7850	– 473	–22	.87	7.1	.2	
2.				112	7850	– 473	–45	.72	6.85	.2	
3.				112	7850	– 473	–67	.58	6.85	.18	
4.				112	7850	– 473	–90	.48	6.95	.22	
5.				112	7850	– 473	Ground	3.85	7.8	.26	
6.				112	7850	– 473	Floating	5.2	6.7	.68	
7.				112	7850	– 473	Floating	4.23			2014
23P	Rerun of 20P but with platinum needle and same P_f and V_N as 22..	Platinum	NaI (20g)/ Glyc. (100 Ml)								
1.				115	7850	– 473	–22	1.43	5.4	.08	1382
2.				115	7850	– 473	–45	1.61	5.5	.07	2008
3.				115	7850	– 473	–67	1.01	5.3	.07	1462
4.				115	7850	– 473	–90	1.01	5.4	.068	1759
5.				115	7850	– 473	Ground	1.13	4.95	.07	879

1

eedle Tests

FOLDOUT FRAME 2

)	I_N (μ A)	I_{EXT} (μ A)	$\left(\frac{\text{ACMR Coul.}}{\text{Kg}}\right)$	I_{SP} (Sec.)	m (lbm/sec.)	$\frac{I_N}{I_C}$ m (lbm/sec)	T (μ lb)	$\frac{I_N}{I_C}$ T (μ lb)	η_b (%)	q/m Coul/Kg	Comments
9			2641	540.2	$.66 \times 10^{-9}$		.356		89.2	2356	Data for 13P → 19P was obtained during continuous run of Hastelloy C Needle for 25½ hour period.
2			2917	546.0	$.47 \times 10^{-9}$		.257		83.8	2444	
8			4163	654.3	$.36 \times 10^{-9}$		.236		83.0	3455	P_f was reduced to 60 MM Hg for 15½ hours (overnight).
6			3698	608.0	$.33 \times 10^{-9}$		.201		82.1	3036	I_c was basically stable but shifted periodically, and showed some evidence of sparking.
8			3998	600.0	$.40 \times 10^{-9}$		.240		71.5	2859	Erosion of the needle did occur but was smoother than with stainless needle.
			3652	553.0	$.60 \times 10^{-9}$		.332		67.0	2447	
2			3074	489.3	$.59 \times 10^{-9}$		.289		62.9	1934	
2.2	1.89×10^{-2}		1329	330.1	1.44×10^{-9}	3.64×10^{-9}	.476	1.20	67.3	894	Screen stand-off distance 1"
1.62	1.89×10^{-2}		1004	282.3	1.38×10^{-9}	3.54×10^{-9}	.390	1.00	65.2	655	
1.99	1.25×10^{-2}		1092	305.4	1.11×10^{-9}	4.02×10^{-9}	.339	1.23	70.1	765	
1.90	2.5×10^{-2}		924.8	274.5	1.26×10^{-9}	4.51×10^{-9}	.347	1.24	67.0	620	
2.8	2.65×10^{-2}		1476	340.0	1.9×10^{-9}	4.19×10^{-9}	.646	1.42	64.5	952	
2.45	2.25×10^{-2}		996.3	286.6	1.55×10^{-9}	5.43×10^{-9}	.444	1.55	67.7	674	
6	.55		2240	476.7	2.11×10^{-9}	5.91×10^{-9}	1.0	2.80	69.2	1550	Screen stand-off distance ¼"
5.8	.52		1677	416.6	$.92 \times 10^{-9}$	7.63×10^{-9}	.383	3.17	70.6	1184	
5.65	.45		1693	425.4	$.87 \times 10^{-9}$	7.34×10^{-9}	.371	3.13	72.9	1234	
5.9	.51		1935	444.6	$.74 \times 10^{-9}$	6.71×10^{-9}	.329	2.98	69.7	1349	
5.65	.45		1739	431.0	1.0×10^{-9}	7.15×10^{-9}	.431	3.08	72.8	1266	
7.1	.2										All glass feed system
6.85	.2										
6.85	.18										Positive overshoot on all but floating point test.
6.95	.22										
7.8	.26										Screen stand-offs ¼"
6.7	.68										
			2014	422.0	4.63×10^{-9}		1.95		54.4	1096	
5.4	.08		1382	422.1	2.28×10^{-9}	8.61×10^{-9}	.96	3.62	79.6	1100	Screen stand-off distance 1"
5.5	.07		2008	484.8	1.77×10^{-9}	6.05×10^{-9}	.857	2.93	72.3	1452	Collector current fairly steady
5.3	.07		1462	438.1	1.52×10^{-9}	7.97×10^{-9}	.667	3.50	81.1	1186	Positive overshoot on all but
5.4	.068		1759	483.4	1.27×10^{-9}	6.80×10^{-9}	.612	3.27	82.0	1442	Test #2.
4.95	.07		879	342.7	2.83×10^{-9}	12.4×10^{-9}	.971	4.26	82.5	725	

Table 1 (continued)

Test #	Purpose of Test	Needle	Propellent	P_f (MM Hg)	V_N (Volts)	V_{EXT} (Volts)	V_{SCR} (Volts)	I_C (μA)	I_N (μA)	I_{EXT} (μA)	$\left(\frac{\text{ACMR}}{\text{Coul.}}{\text{Kg}}\right)$	I_{SP} (Sec.)	(lb
24P	To determine the effect of operating with a metal screen liner in vacuum T,	Platinum	NaI (20g)/ Glyc. (100 Ml)	108	7900	– 473	–22						
25P	Duration run for platinum needle.	Platinum	NaI (20g)/ Glyc. (100 Ml)	107	8200	– 473	–22						
26P	To determine the effect of varying the concentration of NaI solution.	Platinum	NaI (10g)/ Glyc. (100 Ml)										
1.				103	8650	– 473	–22	.09	.31	.1	93.97	124.1	2.1
2.				103	8650	– 473	–45	.09		.1	98.58	125.8	2.0
3.				103	8650	– 473	–67	.09		.1	95.43	121.8	2.1
4.				103	8650	– 473	–90	.08		.1	87.94	123.3	2.0
5.				103	8650	– 473	Ground	.10		.1	99.66	121.2	2.2
27P	To determine the effect of varying the concentration of NaI solution.	Platinum-10% Iridium	NaI (15g)/ Glyc. (100 ML)										
1.				110	8000	– 473	–22	.05	2.4	.11	78.19	114	1.4
2.				110	8000	– 473	–45	.05	2.3	.11	80.95	115.8	1.3
3.				110	8000	– 473	–67	.05	2.5	.11	78.19	114	1.4
4.				110	8000	– 473	–90	.05	2.3	.11	78.19	114	1.4
5.				110	8000	– 473	Ground	.05	2.4	.11	76.3	112.6	1.4
28P	To determine the effect of varying the concentration of NaI solution.	Platinum-10% Iridium	NaI (18g)/ Glyc. (100 ML)										
1.				98	9000	– 473	–22	.65		.19	1468	447.4	.9
2.				98	9000	– 473	–45	.56		.19	1799	481.0	.6
3.				98	9000	– 473	–90			.25			
29P	Test hydrochloric acid as propellent.	Platinum-10% Iridium	HCl (2½ ML)/ Glyc. (100 ML)	107	8000	– 473	–22	.60			71.63	109.1	1.8
30P	Test hydrochloric acid as a propellent.	Platinum-10% Iridium	HCl (34 ML)/ Glyc. (100 ML)										
31P	Test sulphuric acid as a propellent.	Platinum-10% Iridium	H_2SO_4 (10½ ML)/ Glyc. (100 ML)										
32P	Test sulphuric acid as a propellent.	Platinum-10% Iridium	H_2SO_4 (2 ML)/ Glyc. (250 ML)										
33P	Test sulphuric acid as a propellent.	Platinum-10% Iridium	H_2SO_4 (2 ML)/ Glyc. (250 ML)	245	8700	– 473	–90	.48			246.3	204.8	4.3
34P	Test sodium hydroxide as a propellent.	Platinum-10% Iridium	NaOH (1g)/ Glyc. (100 ML)	230	9200	– 473		.45			208.3	181.1	4.76

inued)

FOLDOUT FRAME 2

N (A)	I_{EXT} (μA)	$\left(\frac{ACMR}{\frac{Coul.}{Kg}}\right)$	I_{SP} (Sec.)	m (lbm/sec.)	$\frac{I_N}{I_C}$ m (lbm/sec)	T (μ lb)	$\frac{I_N}{I_C}$ T (μ lb)	η_b (%)	q/m Coul./Kg	Comments
										Very erratic. Test terminated ¼'' stand-off distance from this point on.
										Same needle as in 22P, 23P, 24P.
										Operating conditions varied from those listed.
										Ran smoothly for one day; was spiking next day. Argon ran out third day.
31	.1	93.97	124.1	2.1×10^{-9}	7.25×10^{-9}	.262	.904	91.78	86.25	Very stable operation.
	.1	98.58	125.8	2.0×10^{-9}		.252		89.21	87.94	
	.1	95.43	121.8	2.1×10^{-9}		.253		87.11	83.13	
	.1	87.94	123.3	2.0×10^{-9}		.247		96.84	85.16	
	.1	99.66	121.2	2.2×10^{-9}		.268		82.49	82.21	
	.11	78.19	114	1.41×10^{-9}	67.6×10^{-9}	.161	7.72	100.	78.66	Very stable operation.
	.11	80.95	115.8	1.36×10^{-9}	62.6×10^{-9}	.158	7.27	100.	81.19	
	.11	78.19	114	1.41×10^{-9}	70.5×10^{-9}	.161	8.05	100.	78.66	
	.11	78.19	114	1.41×10^{-9}	64.9×10^{-9}	.161	7.41	100.	78.66	
	.11	76.3	112.6	1.45×10^{-9}	69.5×10^{-9}	.163	7.82	100.	76.83	
	.19	1468	447.4	$.98 \times 10^{-9}$		.437		73.4	1078	Very erratic performance.
	.19	1799	481.0	$.69 \times 10^{-9}$		.332		70.4	1266	Test terminated.
	.25									
		71.63	109.1	1.85×10^{-9}		.202		100.	72.13	Started stable but became very erratic. Bubbles observed at needle inlet.
										Very erratic performance at + and − V_N. Severe needle erosion.
										Very erratic with erosion of needle. Ran with both positive and negative V_N.
										Very erratic with some erosion of needle. Propellent not completely degassed.
		246.3	204.8	4.3×10^{-9}		.88		94.8	233.4	Erratic performance — no needle erosion.
		208.3	181.1	4.76×10^{-9}		.863		82.94	172.8	Fairly stable performance.

Table 1 (continued)

Test #	Purpose of Test	Needle	Propellent	P_f (MM Hg)	V_N (Volts)	V_{EXT} (Volts)	V_{SCR} (Volts)	I_C (μ A)	I_N (μ A)	I_{EXT} (μ A)	$\left(\frac{ACMR}{Coul./Kg}\right)$	I_{SP} (Sec
35P	Test sodium hydroxide as a propellent.	Platinum-10% Iridium	NaOH (2.3g)/ Glyc. (100 ML)									
1.				157	4900	− 473	−22	.30			595.5	21
2.				193	4900	− 473	−22	.52			584.6	22
3.				195	5000	− 473	−22	.28			374.5	18
4.				105	5400	− 473	−22	.39			987.2	30
5.				105	5900	− 473	−22	.59			1390	37
6.				60	6000	− 473	−22	.52			2009	45
7.				35	6300	− 473	−90	.46			3350	59
36P 2.	Test sodium hydroxide propellent at high feed pressure.	Platinum-10% Iridium	NaOH (2.3g)/ Glyc. (100 ML)	109	6000	− 473	−45	.15			286.1	16
37P	Test sodium hydroxide propellent at low feed pressure.	Platinum-10% Iridium	NaOH (2.3g)/ Glyc. (100 ML)									
1.				42	6800	− 473	−45	.15			772.7	300
2.				40	6900	− 473	−45	.46			1879	474
38P	Test sodium iodide propellent at high and low pressures.	Platinum-10% Iridium	NaI (20g)/ Glyc. (100 ML)									
1.				315	8400	− 473	−22	.50			299.3	196
2.				33	9600	− 473	−22	.23			1293	410.
39P	Test first inside tapered needle. (I.T.N.)	Platinum-10% Iridium	NaI (20g)/ Glyc. (100 ML)									
1.				50	6200	− 473	−22 or −45	.49			1281	196.
2.				175	7800	− 473	−22 or −45	1.95			1907	450.
40P	Test effect of smaller diameter extractor. (I.T.N.)	Platinum-10% Iridium	NaI (20g)/ Glyc. (100 ML)									
1.				53	6200	− 473	−22 or −45	.19			2086	448.
2.				177	7800	− 473	−22 or −45	3.25			2703	592.
3.				37	6700	− 473	−22 or −45	.75			2326	525.
41P	Test effect of coating screen and rear assembly with aquadag. (I.T.N.)	Platinum-10% Iridium	NaI (20g)/ Glyc. (100 ML)									
1.				43	7500	− 473	−22 or −45	.33			1110	338.
2.				40	6700	− 473	−22 or −45	.31			992.7	333.
3.				175	7700	− 473	−22 or −45	1.09			680.5	276
42P	Test effect of auxiliary plate on TOF overshoot. (I.T.N.)	Platinum-10% Iridium	NaI (20g)/ Glyc. (100 ML)									
1.				40	6700	− 473	−22	.74			2384	533.
2.				180	7600	− 473	−22	2.72			2191	530.
43P	Retest of 39P (I.T.N.)	Platinum-10% Iridium	NaI (20g)/ Glyc. (100 ML)	42	8200	− 473	−45	.39			2694	604.

ntinued)

FOLDOUT FRAME 2

I_N (μ A)	I_{EXT} (μ A)	$\left(\frac{ACMR}{\frac{Coul.}{Kg}}\right)$	I_{SP} (Sec.)	m (lbm/sec.)	$\frac{I_N}{I_C}$ m (lbm/sec)	T (μ lb)	$\frac{I_N}{I_C}$ T (μ lb)	η_b (%)	q/m Coul./Kg	Comments
		595.5	211.1	1.11×10^{-9}		.235		74.42	443.2	Fairly stable. Large amount of precipitate observed at needle tip after test. No apparent tip erosion.
		584.6	223.5	1.96×10^{-9}		.438		84.44	493.6	
		374.5	180.3	1.65×10^{-9}		.297		84.15	315.1	
		987.2	308.8	$.87 \times 10^{-9}$		.269		86.69	855.8	
		1390	370.6	$.94 \times 10^{-9}$		.347		81.13	1128	
		2009	452.3	$.57 \times 10^{-9}$		.258		82.24	1652	
		3350	590.0	$.30 \times 10^{-9}$		.177		78.0	2613	
		286.1	167	1.16×10^{-9}		.193		78.8	225.4	4 hr. test. Some precipitate on needle but not as much as in 35P.
		772.7	300.0	$.43 \times 10^{-9}$		.129		83.3	643.7	4 hr. test. Some precipitate on needle rim but not as much as in 35P.
		1879	474.7	$.54 \times 10^{-9}$		.256		84.2	1582	
		299.3	196.0	3.68×10^{-9}		.722		74.2	222.1	Erratic. Precipitate on needle but not as much as 35P.
		1293	410.0	$.39 \times 10^{-9}$		.160		65.2	843.0	
		1281	196.0	$.84 \times 10^{-9}$		.310		81.8	1048	Very steady at low pressure; somewhat unsteady at high pressure.
		1907	450.3	2.25×10^{-9}		1.015		66.1	1261	
										Extractor size changed from 7/16" i.d. to .279" i.d.
		2086	448.8	$.2 \times 10^{-9}$		.09		75.5	1575	Erratic performance.
		2703	592.8	2.65×10^{-9}		1.57		80.8	2184	
		2326	525.7	$.71 \times 10^{-9}$		.374		86.0	2000	Positive overshoot on TOF.
		1110	338.1	$.66 \times 10^{-9}$		.22		66.5	738.2	Screen and rear assembly coated with aquadag. Positive overshoot occurred on TOF. .279" i.d. extractor. Erratic performance.
		992.7	333.0	$.69 \times 10^{-9}$		.23		84.7	840.8	
		680.5	276	3.53×10^{-9}		.97		70.4	479.1	
		2384	533.0	$.68 \times 10^{-9}$		.362		85.0	2026	Plate at needle potential located in back of needle assembly. Positive overshoot was eliminated, but effect of plate on field unknown. .279" i.d. extractor.
		2191	530.0	2.7×10^{-9}		1.43		80.1	1755	
		2694	604.9	$.32 \times 10^{-9}$		.193		80.3	2168	Screen and rear assembly coated with aquadag. Data indicated current leak between screen and collector. Large extractor (7/16" i.d.) very stable.

Table 1 (continued)

Test #	Purpose of Test	Needle	Propellent	P_f (MM Hg)	V_N (Volts)	V_{EXT} (Volts)	V_{SCR} (Volts)	I_C (μA)	I_N (μA)	I_{EXT} (μA)	$\left(\frac{ACMR}{Coul./Kg}\right)$	I_{SP} (Sec.)	m (lbm/sec.)
44P	Retest of 39P (I.T.N.)	Platinum-10% Iridium	NaI (20g)/ Glyc. (100 ML)	38	7800	− 473	−45	.56			2888	601.0	$.43 \times 10^{-9}$
45P	Test second inside tapered needle. (I.T.N.)	Platinum-10% Iridium	NaI (20g)/ Glyc. (100 ML)	35	5500	− 473	−45	.29			1474	368.0	$.43 \times 10^{-9}$
46P	Test effect of varying extractor voltage on performance. (I.T.N.)	Platinum-10% Iridium	NaI (20g)/ Glyc. (100 ML)										
1.				57	7800	− 473	−45	.33			989.2	356.1	$.74 \times 10^{-9}$
2.				57	6300	− 780	−45	.39			1824	444.6	$.47 \times 10^{-9}$
3.				57	6400	−1100	−45	.39			1908	443.2	$.45 \times 10^{-9}$
4.				57	6400	−1450	−45	.41			1718	455.6	$.53 \times 10^{-9}$
5.				57	6400	− 780	−90	.30			2501	535.0	$.26 \times 10^{-9}$
47P 2.	Test effect of higher P_f on inside tapered needle performance	Platinum-10% Iridium	NaI (20g)/ Glyc. (100 ML)	90	7700	− 473	−45	1.23			5929	866.9	$.46 \times 10^{-9}$
48P	To test outside-tapered needle.	Platinum-10% Iridium	NaI (20g)/ Glyc. (100 ML)										
1.				89	8100	− 473	−45	.81	20	.48	6508	885.0	$.27 \times 10^{-9}$
2.				95	7200	− 473	−45	1.2	16	.42	5243	823.0	$.5 \times 10^{-9}$
3.				100	7000	− 473	−45	1.16			4202	705.1	$.61 \times 10^{-9}$
4.				100	6000	− 473	−45						
5.				98	7300	− 473	−45	.80	15	.4	3915	714.3	$.45 \times 10^{-9}$
6.				98	5900	− 473	−45	.59	5	.16	1331	368	$.98 \times 10^{-9}$

ontinued)

FOLDOUT FRAME 2

I_N (μ A)	I_{EXT} (μ A)	$\left(\frac{\Delta CMR}{\frac{Coul.}{Kg}}\right)$	I_{SP} (Sec.)	m (lbm/sec.)	$\frac{I_N}{I_C}$ m (lbm/sec)	T (μ lb)	$\frac{I_N}{I_C}$ T (μ lb)	η_b (%)	q/m Coul./Kg	Comments
		2888	601.0	$.43 \times 10^{-9}$		.259		79.2	2287	Same as 43P but without aquadag. Very stable.
		1474	368.0	$.43 \times 10^{-9}$		.158		78.8	1162	Erratic performance. Residue buildup at needle tip. Positive overshoot on TOF.
		989.2	356.1	$.74 \times 10^{-9}$		.262		79.6	787.4	Caked-up deposit around rim of needle.
		1824	444.6	$.47 \times 10^{-9}$		.210		83.4	1521	
		1908	443.2	$.45 \times 10^{-9}$		.200		78.0	1488	
		1718	455.6	$.53 \times 10^{-9}$		.240		91.5	1572	
		2501	535.0	$.26 \times 10^{-9}$		.139		84.0	2101	
		5929	866.9	$.46 \times 10^{-9}$		.397		79.8	4731	Stable performance at P_f = 90 MM Hg
20	.48	6508	885.0	$.27 \times 10^{-9}$	6.67×10^{-9}	.239	5.90	69.7	4536	Performance not very stable at V_N = 8 kv. Stable performance at V_N = 6 kv.
16	.42	5243	823.0	$.5 \times 10^{-9}$	6.66×10^{-9}	.412	5.50	85.7	4493	
		4202	705.1	$.61 \times 10^{-9}$		.429		81.9	3441	
15	.4	3915	714.3	$.45 \times 10^{-9}$	8.45×10^{-9}	.322	6.05	86.5	3386	
5	.16	1331	368	$.98 \times 10^{-9}$	8.30×10^{-9}	.360	3.05	83.6	1113	

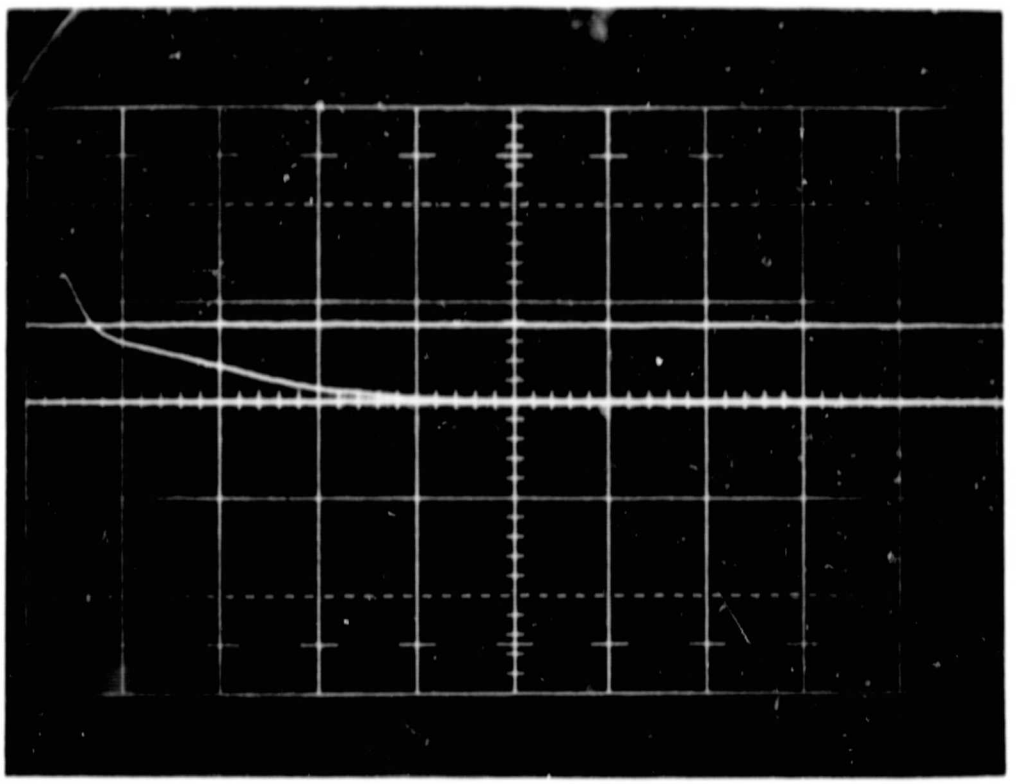

Figure 5. Positive overshoot on TOF trace.

data-reduced flow agreed generally within 20% of the calculated flow (by Poiseuille's equation), it is assumed that the other TOF data-reduced values are of reasonable accuracy.

Another problem area is one of back bombardment of the secondary electrons upon the firing source. One purpose for the extractor is to prevent this back bombardment but, in spite of this, a certain amount of back bombardment can occur. If this becomes significant an error will result in the needle current reading. Essentially, the needle current will assume a value higher by the amount of secondary electrons absorbed. In addition, tar like deposits have been reported[1] presumably due to this back bombardment.

A third effect, difficult to prove experimentally, is eratic performance due to back bombardment. It is possible that this occurrence could disrupt the meniscus at the firing surface causing unstable particle generation.

A thorough theoretical analysis of the secondary emission phenomenon within the vacuum chamber would be extremely complicated, and undoubtedly of questionable validity. Therefore, in this program a series of tests was run with the goal of determining test operating conditions to minimize secondary effects, and, to some degree, the error in the final data caused by secondary emission effects. The tests are designated by numbers 1P to 48P where P stands for preliminary.

All data was reduced from the TOF traces using the computer data reduction technique described earlier in this report.

1. Screen Voltage Variation

Tests 20P to 23P were conducted for the purpose of determining the effects of screen voltage and its distance from the collector on the secondary electron omission.

During test 20P all operating conditions were held constant except suppressor screen voltage. This same procedure was then followed for test 21P, except that the screen stand-off distance was reduced from 1 inch to 1/4 inch.

Figures 6 and 7 are plots of various currents and performance parameters as computed from the TOF curves vs. suppressor screen voltage for tests 20P and 21P.

For both tests the collector current decreases as the suppressor voltage increases negatively. Thus, the net flow of electrons from the collector decreases, and it is reasonable to assume that this decrease is due to suppression of secondary electrons initiated at the collector.

It is also interesting to note that with the 1/4" stand-off distance (test 21P), the final value of collector current is reached at a lower absolute value of negative voltage.

In both tests 20P and 21P the screen current increases as the screen potential increases negatively showing that this increase can be caused by a combination of the net flow of electrons from the screen increasing and an increased number of positive particles hitting it. It is reasonable to assume that part of this net electron flow increase from the screen is due to the suppression of the secondary electrons from the collector which would otherwise come back to the screen.

It should also be noted from Figures 6 and 7 that when both the screen and collector are grounded, their currents are about equal. This is as expected because the transmissivity of the screen is about 50%.

The needle current for test 20P decreases and for test 21P stays the same as the screen voltage increases negatively. The decreasing needle current means that either the net flow of electrons into the needle decreases or the net flow of positive particles from the needle decreases. A reasonable explanation for this result is that the increase in negative screen voltage decreases the secondary electron flow from the collector to the needle. Possibly this effect was obscured by the higher needle current measurements obtained during test 21P.

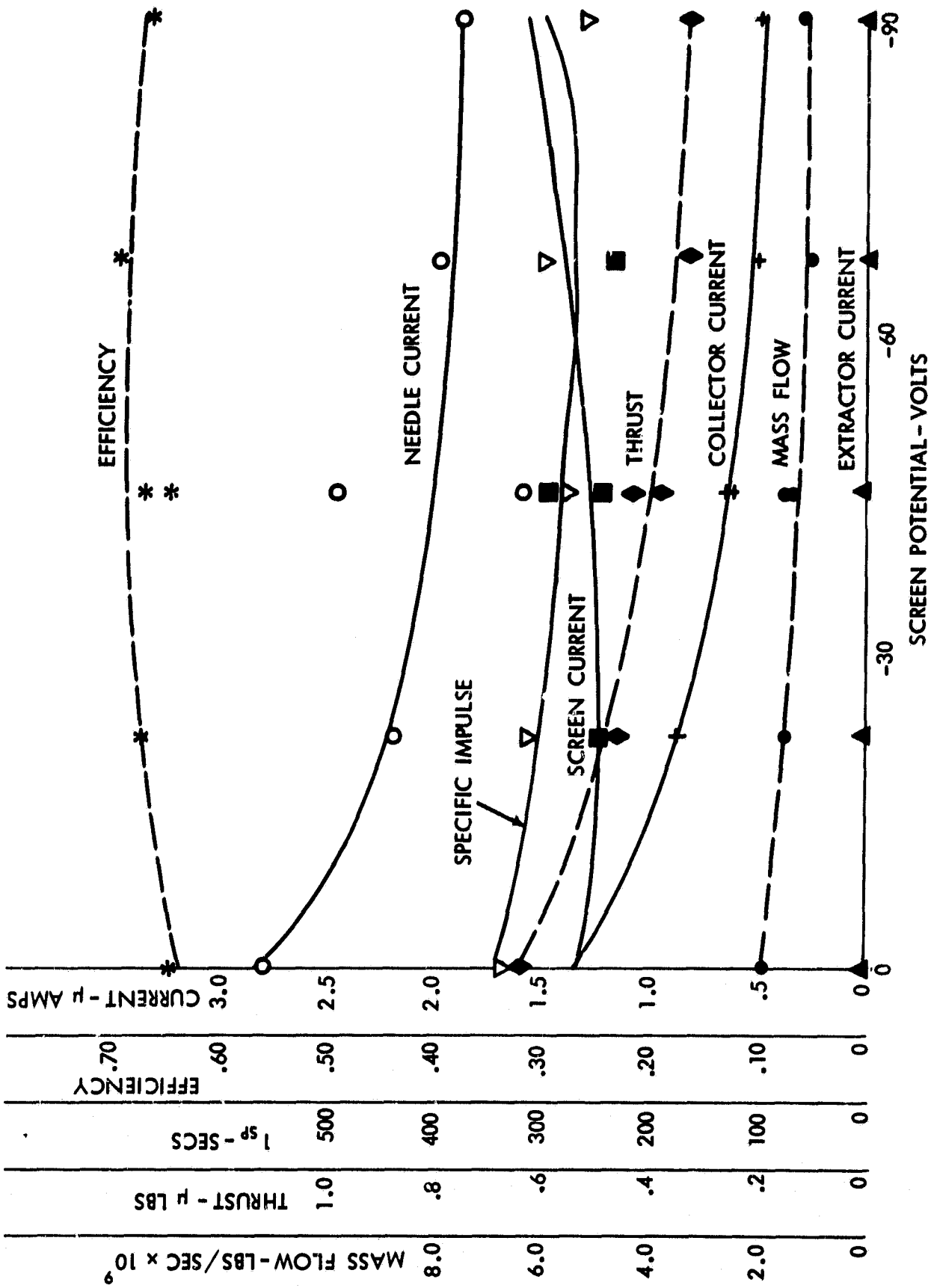

Figure 6. Test 20P curves.

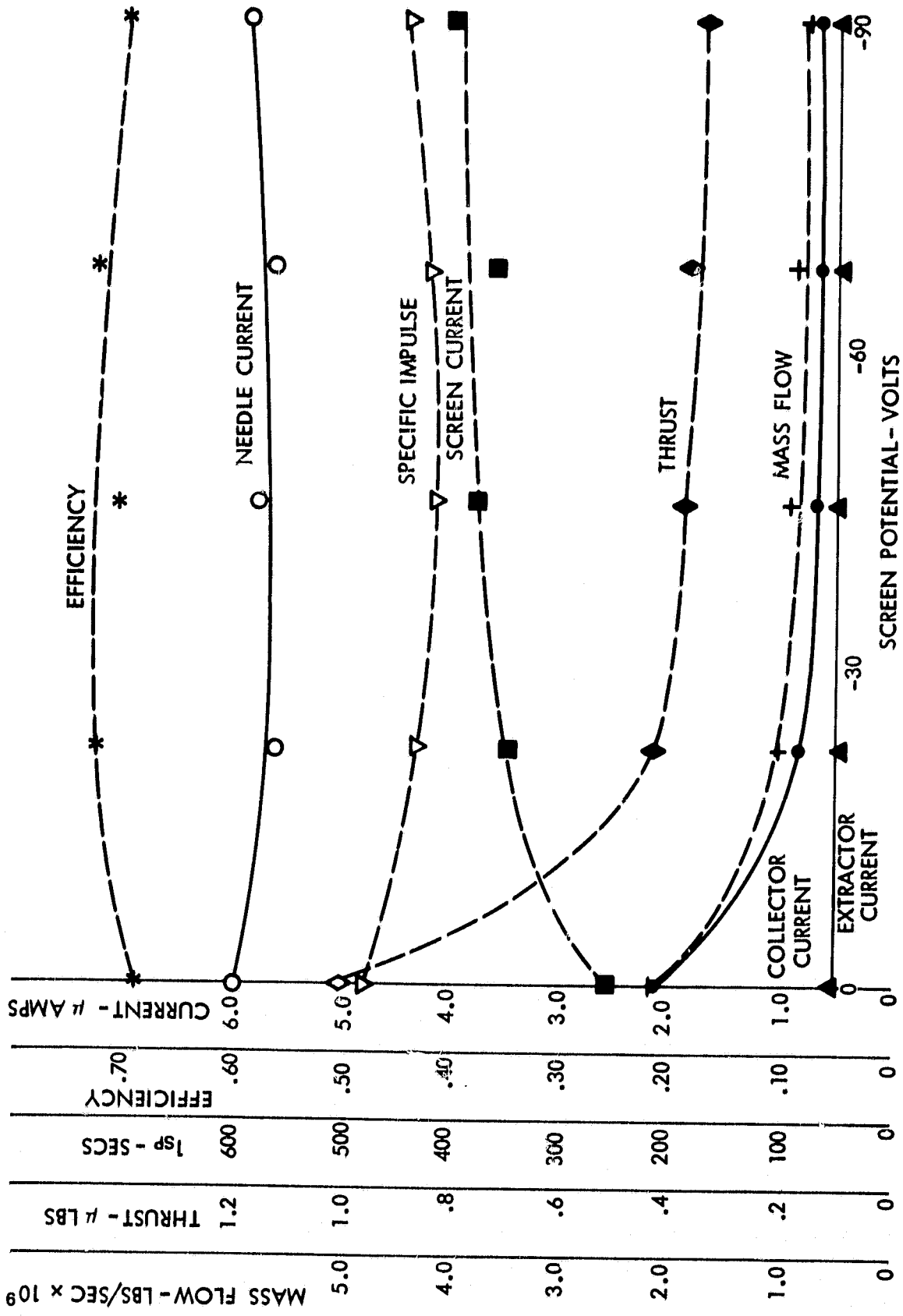

Figure 7. Test 21P curves.

The influence of suppression screen voltage on the needle performance parameters computed from the TOF curves can best be explained with reference to Figure 8a, which shows the TOF traces from test 20P for a suppressor screen voltage of both -90V and ground potential.

As noted previously, because of secondary emission effects, the steady state collector current with a suppressor screen voltage of -90V is less than when the screen is at ground potential. After the zap, however, as the faster colloid particles discharge to the collector, secondary electron effects become less and less significant. Thus, the two curves in Figure 8b eventually coincide, with the total current decay time being the same.

In the TOF data reduction computations,

$$m \propto \int i\, t\, dt \ .$$

Thus, it is seen from Figure 8b that as the screen voltage increases negatively, m decreases. This variation is illustrated in Figures 6 and 7.

The variation of the total flow with screen voltage depends on the ratio of I_N/I_c, and thus is difficult to anticipate. From Table 1 it is seen that the maximum variation of the calculated m is 35% (based on maximum value) for test 20P and 19% for 21P. (It is possible that some of this variation results from a change in the needle tip configuration due to erosion during the test.)

The thrust due to the particles that reach the collector is proportional to

$$\int i\, dt \ .$$

Hence, it would be expected that the calculated value of T decreases as the suppressor screen becomes more negative. Again, this relationship is illustrated in Figures 6 and 7.

The total thrust is equal to $\left(I_N/I_c\right)T$. From Table 1 the maximum variations of the calculated value of thrust with suppressor screen potential is 35% for test 20P and 12% for Test 21P.

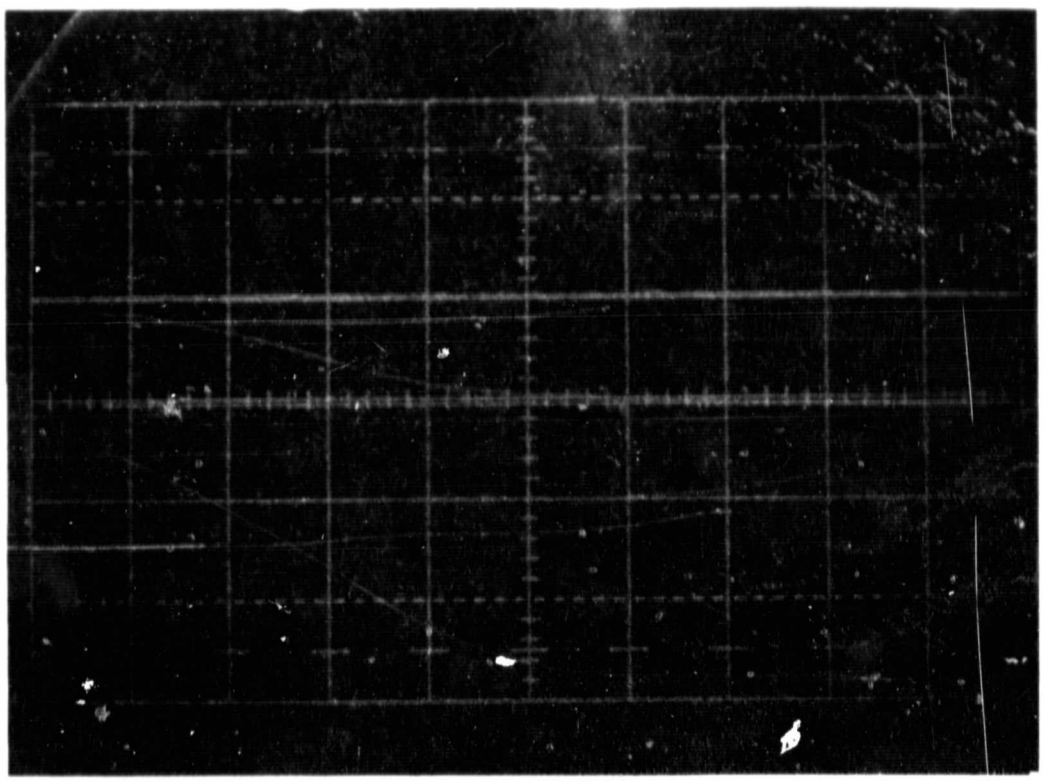

SWEEP =
20 μ sec / cm

VERTICAL =
0.481 μa / cm

V_{scr} = - 90

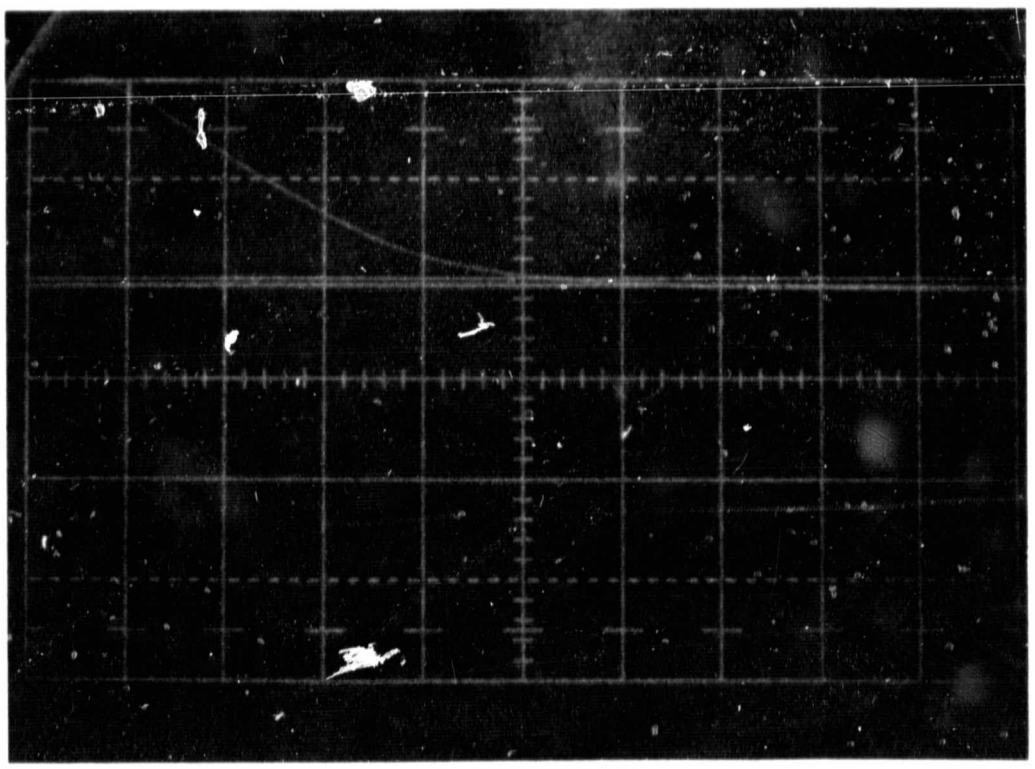

V_{scr} = GROUND

Figure 8a. TOF curves of test 20P for -90 and and ground screen potentials.

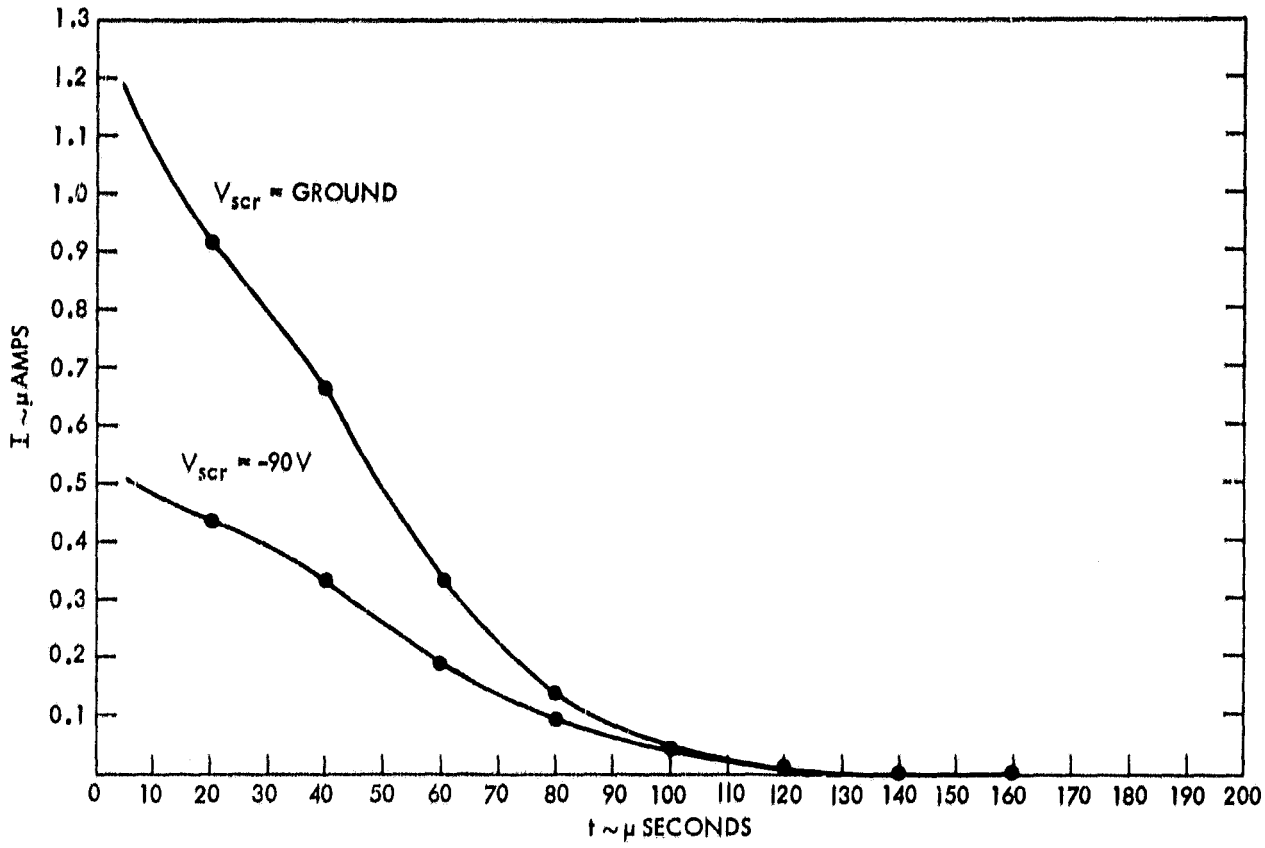

Figure 8b. TOF curves of test 20P for -90 and ground screen potentials.

The variation in the calculated value of specific impulse (proportional to T/m) with suppressor screen potential is shown in Figures 6 and 7. It is seen that the maximum variation in the calculated specific impulse is 19% for test 20P and 12% for test 21P.

Finally, from Table 1, the calculated beam efficiency, which depends on all of the above parameters, has a maximum absolute variation with the suppressor screen voltage of 6% for test 20P and 4% for test 21P.

It was concluded from the above tests that the suppressor screen stand-off distance should be 1/4" and the negative voltage should be at least -22V. This will ensure that the secondary electron emission from the collector is suppressed. Furthermore, from Figures 6 and 7, the calculated values of the performance parameters will have reached their final values. Thus, if there is an error due to secondary emission effects, it is at least constant for a screen -22 or greater (negatively).

The relatively small variation of specific impulse and efficiency with screen voltage is encouraging. From these tests it appears that the calculation of these two parameters may not be greatly influenced by secondary electron effects.

It should be noted, however, that as thruster configurations are changed a check will be made periodically to be certain that maximum secondary suppression is being maintained.

2. Carbon Coating Tests

In an attempt to prevent secondary electron emission in the vacuum chamber, two tests (41P and 43P) were conducted with the suppressor screen and rear assembly coated with Aquadag (carbon dissolved in water).

Examination of the TOF curve for test 41P showed no significant reduction in the positive overshoot. Furthermore, needle performance during the test was as erratic as during test 40P, which was run with the same operating conditions but without the Aquadag.

During test 43P negative collector currents were observed. Various tests were run to determine the reason for this strange performance. One was to keep everything constant except screen voltage. This was increased negatively to -90V in four steps. In this progression, it was observed that the collector current became increasingly negative. It appeared that secondary electrons were bombarding the collector causing this negative current. Another test (44P) was run after removing all traces of Aquadag and cleaning the chamber. It should be noted here that the Aquadag had become quite hard and flaky. This test showed that the collector currents were now reading positive and normally. Apparently, either the Aquadag degraded causing excessive electrons to be emitted or a current leak developed between the screen and collector.

It was concluded that the use of Aquadag had no beneficial effects.

3. Auxiliary Plate

A test was run with an auxiliary extractor plate attached to the needle holder and operated at needle potential. This was an attempt to reduce secondary electron effects by having this plate serve as an electron collector.

The TOF curves for this test (42P) had no positive overshoots for the same test conditions as test 41P. Hence, it appears that the auxiliary plate did have an effect in suppressing secondary electron effects. However, because of the unknown effect of the plate on the electric field around the needle, this method was not adopted as part of the test procedure.

4. Screen Liner

A test was run with a grounded metal screen liner in the vacuum chamber, with provisions for voltage biasing (24P). Extremely erratic performance occurred during this test at all liner biasing voltages, and a TOF curve could not be obtained. Thus, it was concluded that the screen liner was detrimentally affecting the secondary emission problems.

5. Extractor I.D. Variations

Tests 39P and 40P were conducted under the same conditions except 39P had a .437 inch I.D. extractor and 40P had a .274 inch I.D. extractor. The purpose of this was to determine if performance could be improved by getting improved field shaping with the smaller I.D.

Results of the testing showed that the smaller I.D. extractor improved specific impulse, however, performance was erratic and a positive overshoot on the TOF resulted. The larger I.D. extractor produced more stable results with no TOF overshoot.

Test 44P was a rerun of 39P to determine if feed pressure and voltage could be changed to a level where the specific impulse and ACMR would be equal to that attained in test 40P. As shown by the results in Table 1, both the ACMR and specific impulse obtained by this test were higher than that obtained in test 39P.

From the above results it was concluded that the smaller extractor size did not significantly improve specific impulse or ACMR. Moreover, the erratic performance which results from running the smaller extractor made its use unwise.

It is interesting to note Figure 9, obtained from Reference 5, which is a plot of a function proportional to the field force on the needle tip vs. extractor diameter-to-needle ratio, as obtained from a theory presented in the reference. The two extractor sizes tested in this program fall on the asymtotic portion of the curve. Thus, by this theory no change in performance (ignoring secondary emission effects) would be expected between these two extractor sizes.

6. Extractor Voltage Variations

Test 46P was run in order to determine the effect of varying extractor voltage, while holding all other operating parameters constant. Figure 10, which is a plot of specific impulse vs. extractor voltage, shows the results of this test.

It can be concluded from Figure 10 that the variation in specific impulse that occurred appears to be due to a change in needle tip shape caused by

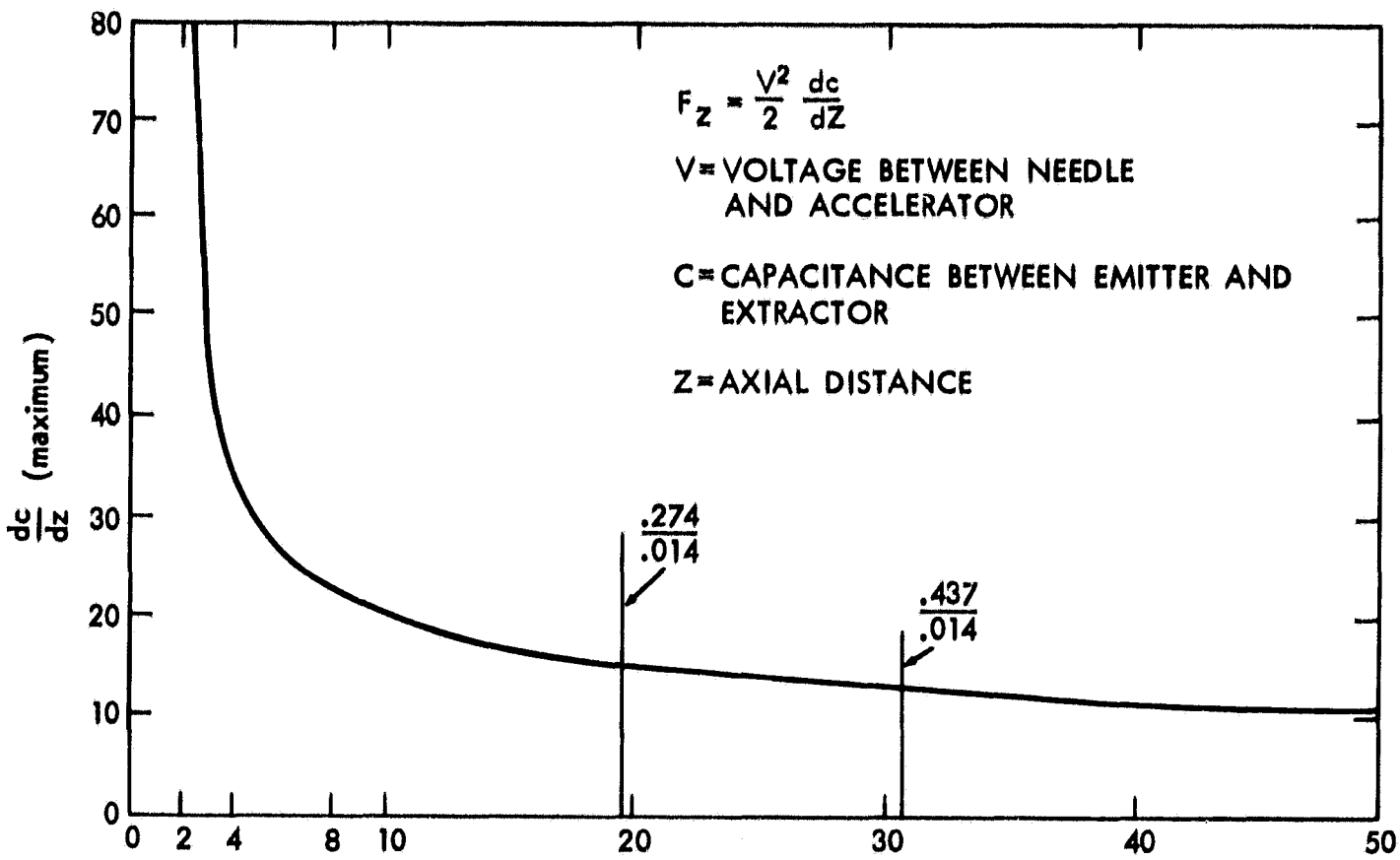

Figure 9. Force function vs. aperture to needle diameter ratio curves from Reference 5.

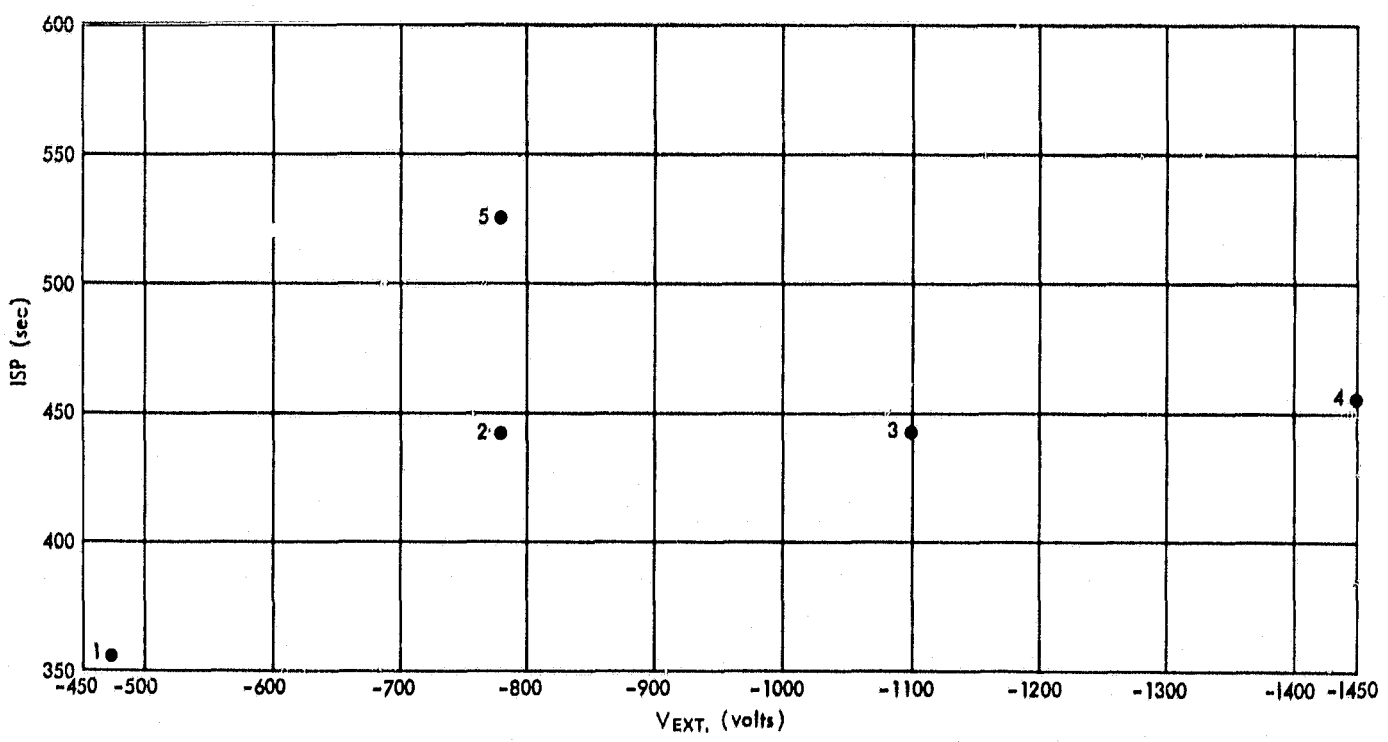

Figure 10. I_{sp} vs. Vext (46P).

deposit build-up rather than extractor voltage, as evidenced by the increase of specific impulse and the decrease of flow rate with time (Table 1).

B. Propellant Variations

A series of tests was run in order to determine the performance characteristics of several different propellant combinations. A summary of the results of these tests is contained in this section.

All of the tests up to 38P which included the propellant variation testing were run with a needle having approximately a .001 inch rim radius, as opposed to a .0001 inch rim radius employed in later testing. As will be discussed later, much of the difficulty encountered with stability and needle tip deposits was considerably reduced with the .0001 inch radius design.

1. Hydrochloric Acid - Glycerol Test

Test 29P employed a propellant consisting of a solution of 2-1/2 ml of a 38% solution of hydrochloric acid and 100 ml of glycerol. The resistivity of the propellant measured 3100Ω-cm at 25°C before the degassing procedure, and 7100Ω-cm after the test. Also, the test was run without fully dehydrating the propellant because the high partial pressure of HCl made dehydration without driving off a substantial amount of HCl extremely difficult.

Sporadic collector current pulsing with a zero D.C. level was observed during this run. The test was eventually terminated because of the collection of bubbles at the needle inlet.

Test 30P was run with a propellant consisting of 34 ml of 38% hydrochloric acid solution and 100 ml of glycerol. The resistivity of the propellant before degassing measured 88Ω-cm at 25°C. Various values of positive and negative needle voltage (in the 4-5 KV range) were applied during this test, but in all cases erratic performance and sporadic pulsing of collector current was observed. In addition, severe erosion of the needle occurred, as shown in Figure 11, even though the total duration of the test was only 20 minutes.

2. Sulfuric Acid - Glycerol Test

A propellant of 10-1/2 ml of 98% solution of sulfuric acid and 100 ml of glycerol was used for this test. The resistivity was 450Ω-cm at 31°C before degassing and 800Ω-cm at 26°C after the test.

Performance during these runs was very erratic for both positive and negative voltages with collector current pulses in the range of 12 microamps. Also, at negative needle voltages a bright glow was observed at the needle tip. During test 31P, as in the tests with the hydrocholoric acid - glycerol propellant combination, severe needle tip erosion occurred. This is shown in Figure 12.

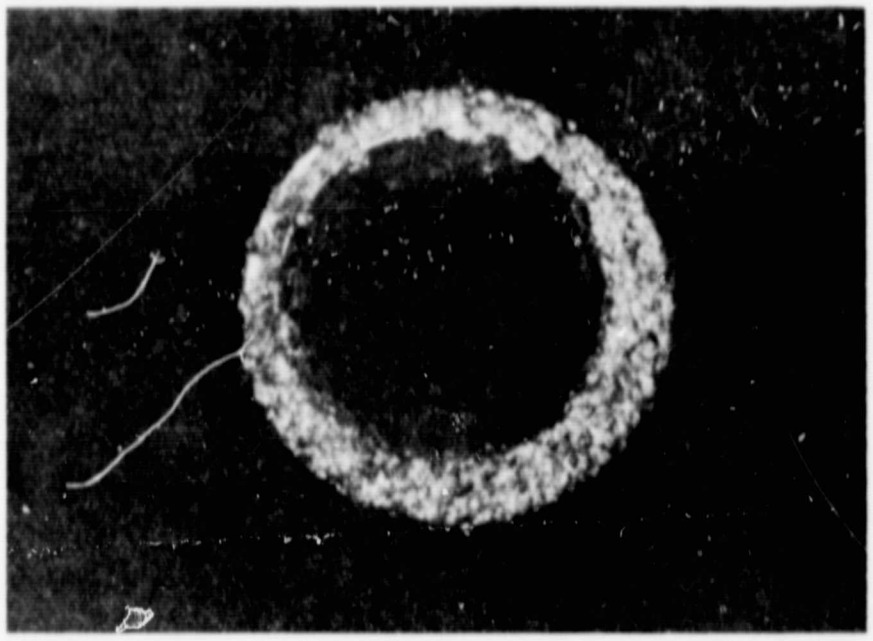

Figure 11. Needle tip after HCl–glycerol test (30P).

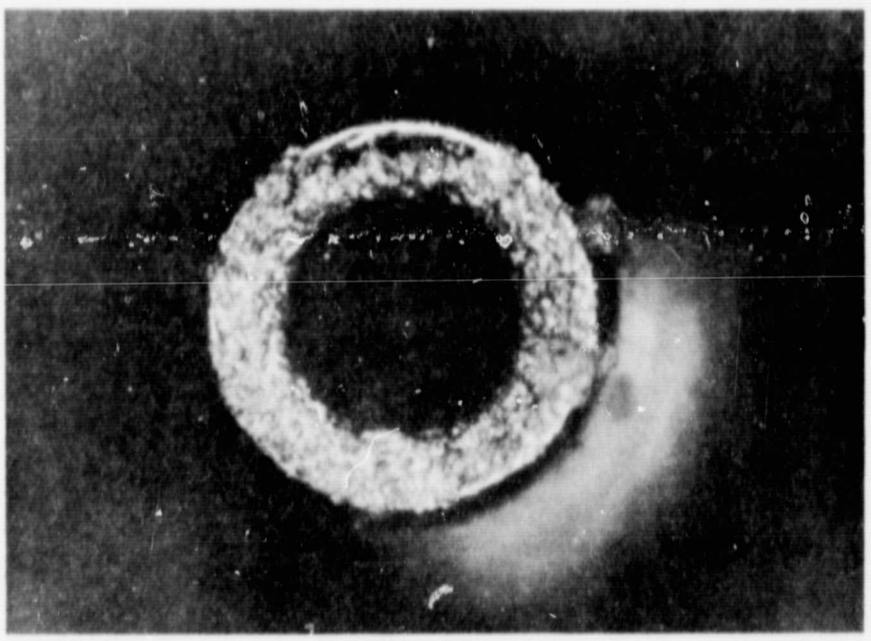

Figure 12. Needle tip after H_2SO_4–glycerol test (31P).

Test 32P was run with a propellant combination of 2 ml of 98% sulfuric acid to 250 ml of glycerol. The resistivity before degassing was 3600Ω-cm at 26.5°C.

The steady state collector current for this test was approximately .05 ua at +6 KV, and, again was extremely erratic. It was thought that this erratic needle performance was due to some water which might have remained in the propellant

during the degassing process. This would follow from the observation that the feed line system was only pumped down to 55 microns Hg prior to the test instead of the usual 15 to 20 microns.

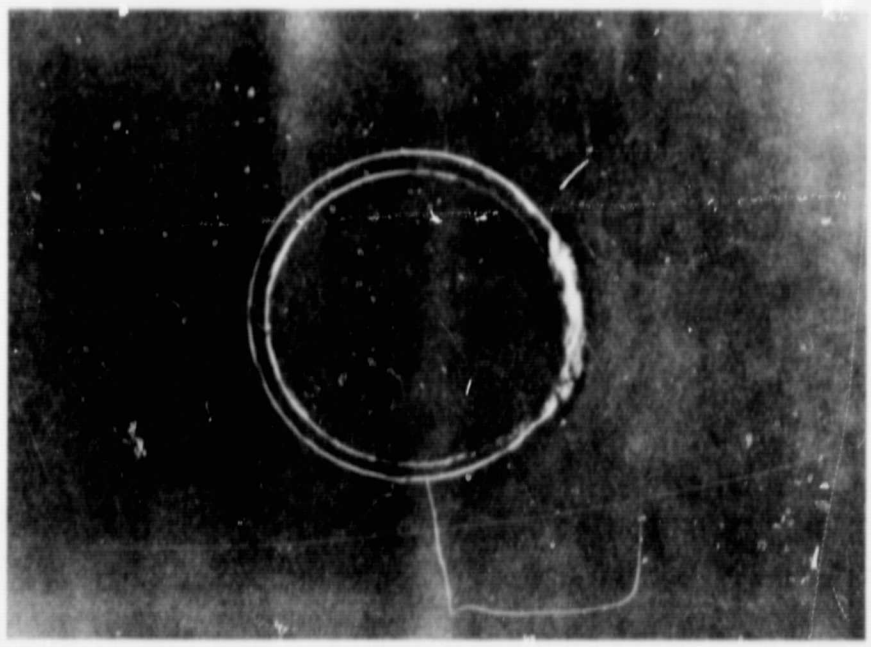

Figure 13. Needle tip after H_2SO_4–glycerol test (32P).

Examination of the needle after the test showed indications of erosion (Figure 13), but at a much reduced level as compared to tests 30P and 31P. Since the needle was not run at negative potential during this test, it is felt that this reduced erosion was an indication that most of the erosion in the previous tests occurred during negative needle voltage operation, when the bright glow at the needle tip was observed.

Test 33P was run with the same propellant batch as 32P, but with the feed line pumped down to 15 microns prior to the test. The resistivity measured after the test was 3400Ω-cm at 26°C.

Erratic performance again occurred during this test; however, a TOF trace was able to be taken (Table 1). There was no needle erosion during this test, again indicating that the erosion during tests 30P and 31P occurred primarily at negative needle voltage. A micro-photograph of the needle tip taken after test 33P is shown in Figure 14.

3. Sodium Hydroxide - Glycerol Tests

Test 34P employed a solution of one gram NaOH to 100 ml of glycerol. The resistivity of this solution was 4780Ω-cm at 26°C before degassing, and 4300Ω-cm at 28°C after the test.

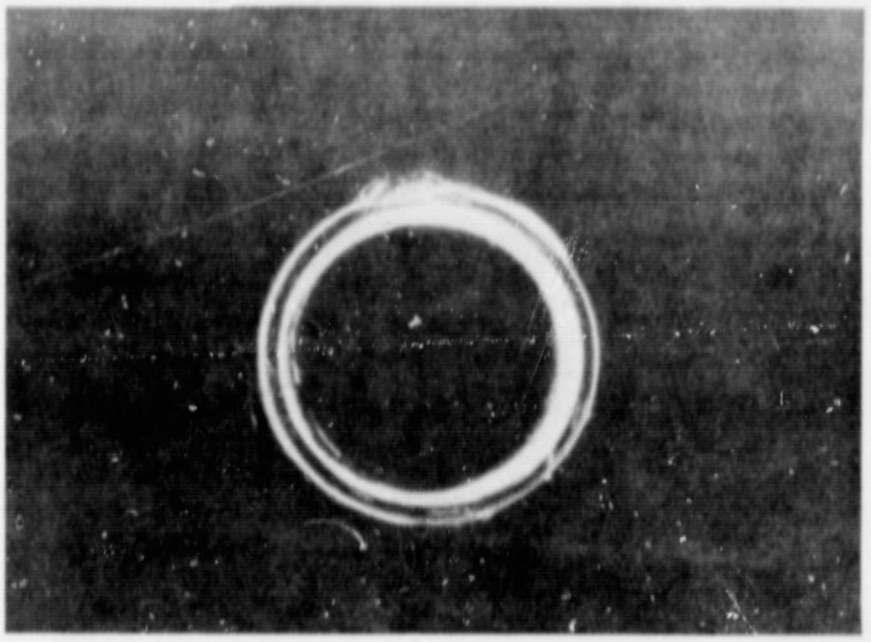

Figure 14. Needle tip after H_2SO_4–glycerol test (33P).

After some initial instabilities the test ran fairly stable, with the performance parameters as shown in Table 1. Since the specific impulse of this propellant combination was low, it was decided to run the next test (35P) with a higher concentration of NaOH in the propellant.

Before discussing test 35P, it is interesting to note that one experiment that was tried during this test was to move the needle such that it was visible in front of the extractor in one case and visible behind it in the other. No difference in steady state collector current was observed.

Test 35P employed a propellant solution of 2.3 grams NaOH to 100 ml of glycerol. The resistivity of the solution measured 2130Ω-cm at 28°C before the degassing process and 4250Ω-cm at 23°C after the test.

The thruster exhibited fairly stable operation with this propellant. Consequently, over a period of about six hours the needle was operated at various combinations of feed pressure and voltage. As shown in Table 1, a specific impulse range of from 211 to 583 seconds was obtained during this period.

Examination of the needle after the test showed a collection of crystalline particles at the needle tip, as shown in Figure 15. It was thought that these particles consisted of sodium hydroxide which precipitated out of the solution as evaporation of glycerol occurred at the needle tip. If this were true it would be expected that at lower flows, and hence larger needle tip residence time for each fluid particle, the rate of sodium hydroxide precipitation would be greater than

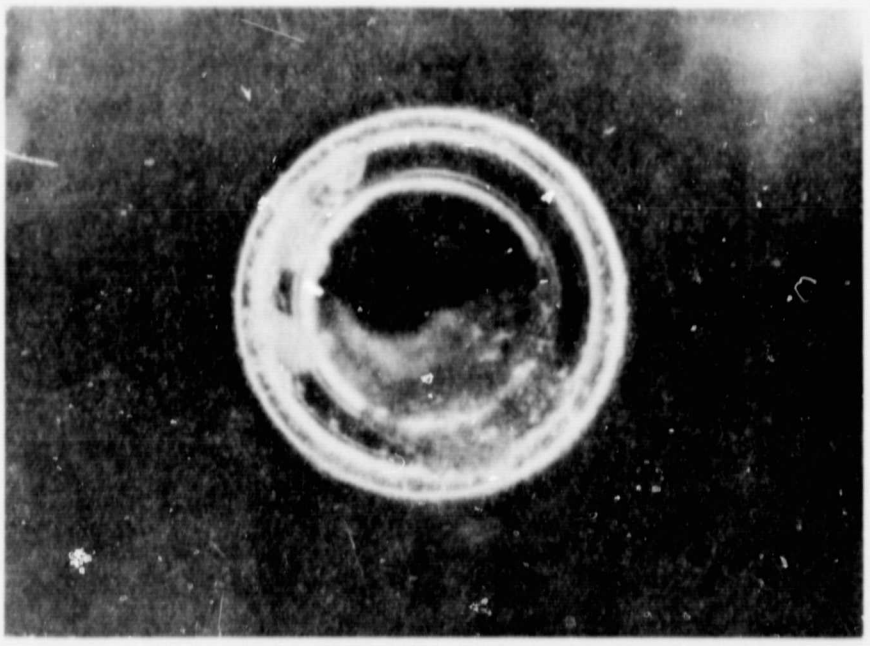

Figure 15. Needle tip after HaOH–glycerol test (35P).

at higher flows. Thus, it was decided to run two sodium hydroxide - glycerol propellant tests for the same length of time, but with different feed pressures. The needle tip would then be examined to determine if the particle precipitation occurred to a higher degree during the lower feed pressure test.

Tests 36P and 37P were both run with the 2.3 grams NaOH - 100 ml glycerol propellant combinations, with a resistivity before degassing of 3100Ω-cm at 24°C. The same needle was used for both tests and was cleaned before each.

Examination of the needle tip after these two tests showed the same deposit as in Figure 15, but to a lesser degree, with no discernable difference in the amount of precipitate between the two tests. Thus, the amount of remaining precipitate was not a visible function of the propellant flow as previously speculated. The composition of these precipitates remained unknown.

4. Sodium Iodide - Glycerol Test

Table 1 shows that a number of tests with the .001 inch radius needle were run with a NaI - Glycerol propellant combination. Some of the more significant tests were 26P-28P which shows that increasing the concentration of NaI increases the specific impulse but results in less stable operation. In general NaI resulted in better stability and performance than the other propellant combinations.

At the end of this series of tests it was obvious that sulfuric acid and hydrocholoric acid were not very good propellant doping agents. The sodium

hydroxide - glycerol propellant resulted in fairly stable performance with a reasonable good specific impulse for the needle voltage applied, but because of the needle tip precipitation problem it was decided to use the sodium iodide - glycerol combination as the propellant for subsequent needle tests.

C. Needle Geometry Variations

Figure 16 shows the approximate dimensions of the three different needle geometries tested during this program. In comparing the performance of these three configurations it is concluded that both the internal and external tapered designs exhibited superior specific impulse and ACMR as compared to the broad radius needle (Figure 16a), with little difference in beam efficiency. For example, both tests 47P (inside taper) and 48P (outside taper) exhibited a specific impulse of about 870 seconds, which was higher than could be achieved during any of the .001 inch tip radius needle tests (13P-38P). This result is expected since the smaller needle tip radius produces a larger electric field concentration at the tip.

The collector current for both the internal and external tapered needle tests (39P, 44P, 48P) was more stable than during any of the .001 inch needle tests.

There was no significant difference in the performance or stability between the internal and external tapered needles; however, pre-test and post-test cleaning of the needle was easier with the outside tapered design.

It should be noted that since generally better performance was obtained with the thin rimmed needles it is possible that some of the particle precipitation problems associated with the earlier sodium hydroxide-glycerol tests could have been reduced or eliminated by using these needle geometries. However, because of the generally successful performance of the sodium iodide - glycerol propellant in these tests no additional propellant evaluation testing was conducted.

D. Needle Material

The following needle materials were tested during this program:

Material	Tests
Stainless Steel	1P-13P - Results not shown in Table 1
Hastelloy C	14P-20P
Platinum	21P-26P
Platinum - 10% Iridium	27P-48P

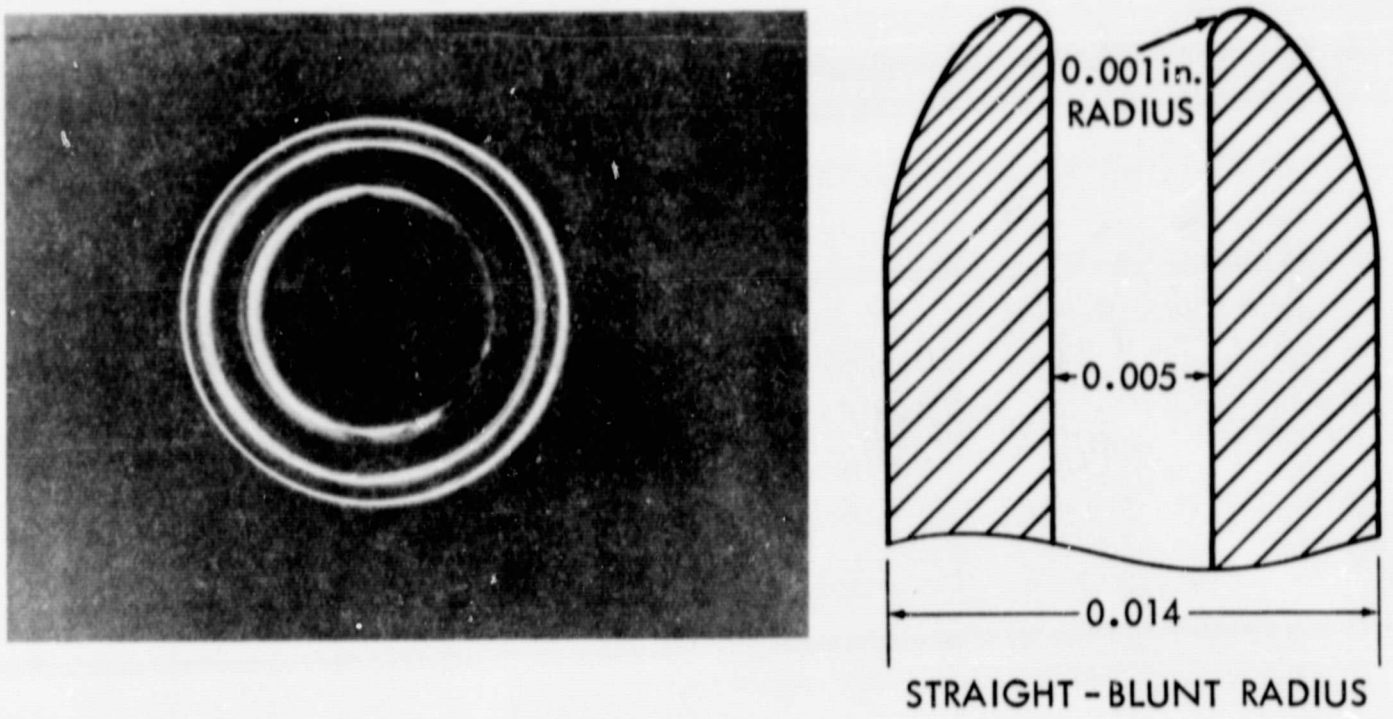

Figure 16a. Needle geometries tested.

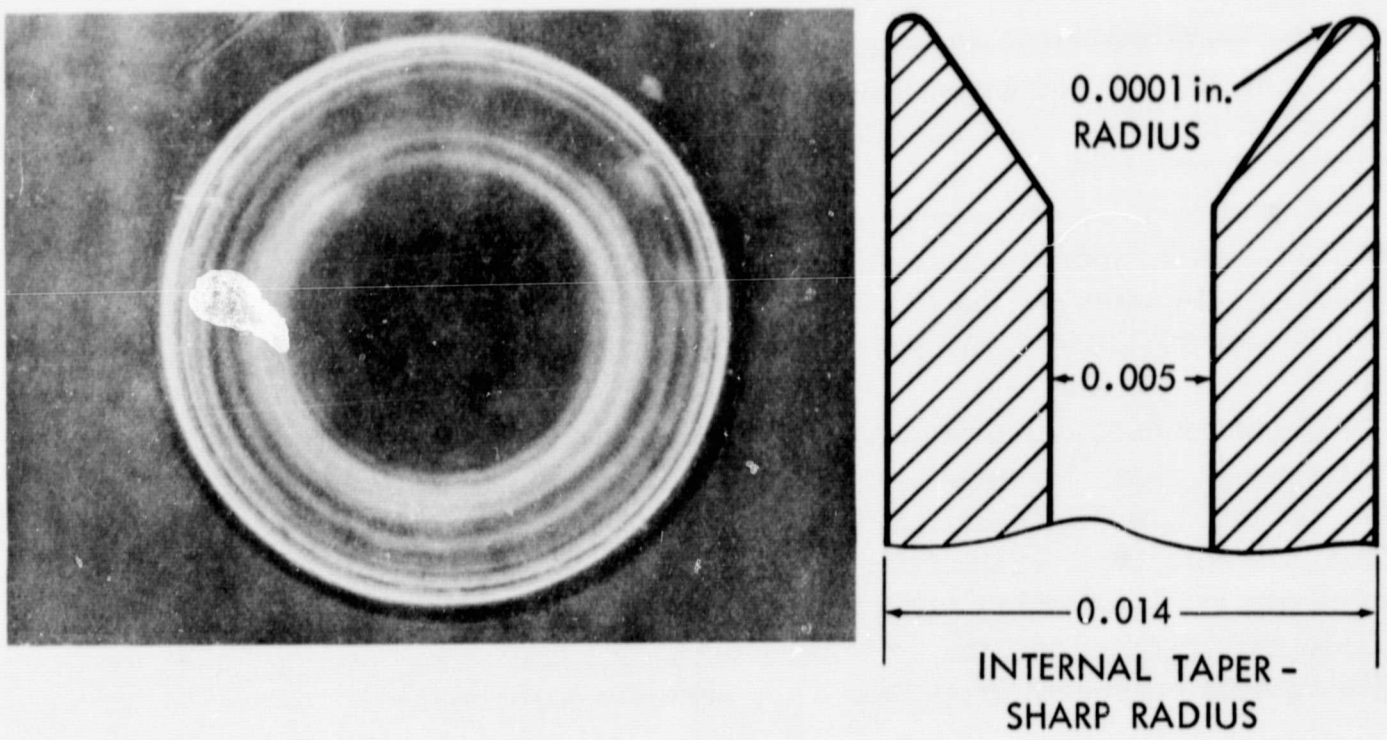

Figure 16b. Needle geometries tested.

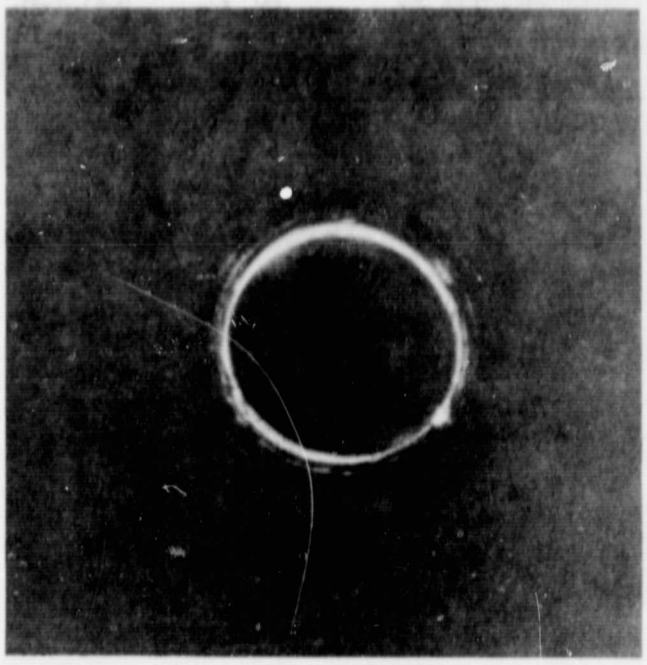

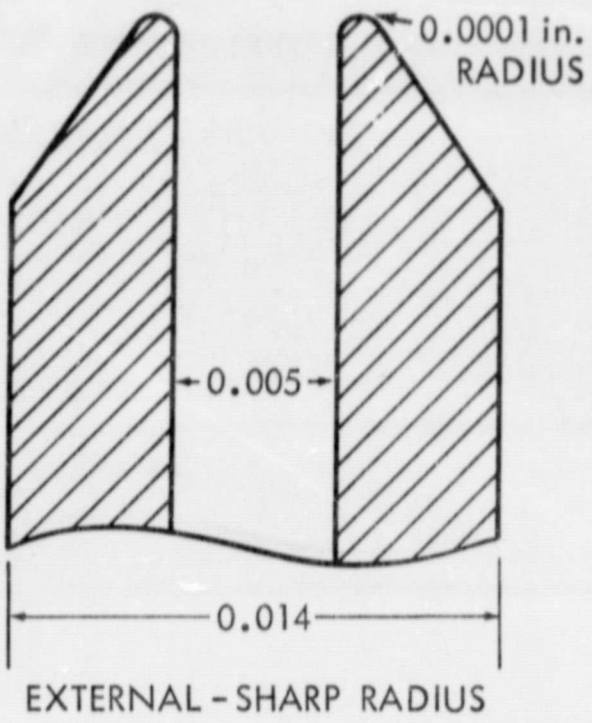

Figure 16c. Needle geometries tested.

The stainless steel needles exhibited a severe needle-tip erosion and pitting when run with the sodium iodide - glycerol propellant combinations. Therefore, the use of stainless steel needles was abandoned early in the program.

Hastelloy C was then employed as a needle material. Erosion again occurred with the sodium iodide - glycerol combinations, but at a reduced rate and with no pitting. In addition, the Hastelloy C needles were run for 24 hour periods with reasonably good performance.

Tests conducted with a pure platinum needle resulted in little or no erosion of the needle tips. However, the softness of pure platinum made needle fabrication extremely difficult and needle damage a likely occurrence during handling. Thus, the remainder of the tests were run with a platinum 10% iridium alloy, which was considerately easier to work, and equally resistant to erosion. Tests 27P to 48P resulted in little or no erosion of the needle tip, except when run with an acid - glycerol propellant as previously described.

MATERIAL TESTING

When considering the process by which charged particles are formed and moved from the thruster to a collector an analogy can be made between this and an electrochemical process. Figure 17 shows a schematic representation of the colloid firing process and an electrochemical process.

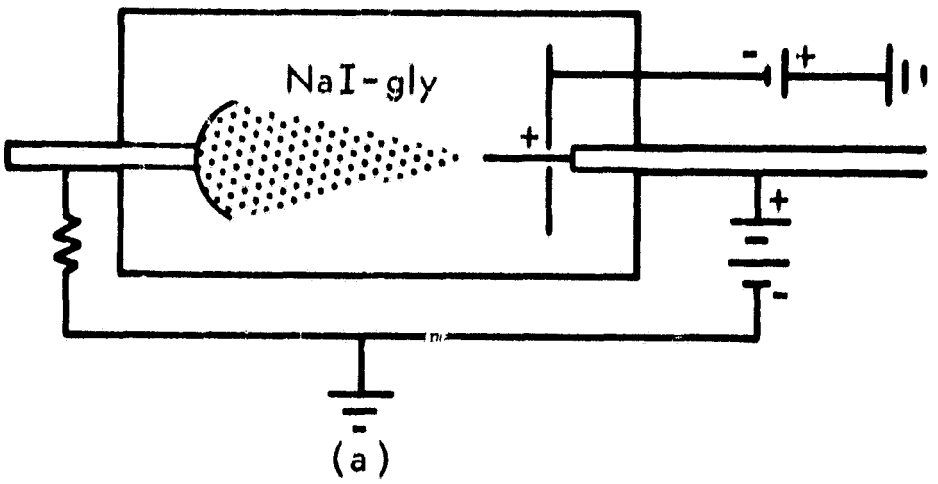

Figure 17. Electrochemical analogies.

The particular analogy that was formed was the relationship of current flow and the reaction occurring at the anodes. In Figure 17a the anode is taken as the needle and the cathode as the collector. The transfer medium is the charged particle flow between the needle and collector. In Figure 17b the anode is the metal to be tested and the cathode is a stable metal such as platinum. The transfer medium is the propellant combination to be tested.

Considering only stable operating conditions of the needle setup (i.e. no arcing or tip glowing) it was found that propellant breakdown and needle erosion performed proportionately to the electrochemical analogy. Because the electrochemical current flow was much higher than the needle condition (milliamps vs. microamps) erosion and propellant breakdown was more rapid, therefore, it was decided to utilize this method to evaluate the stability of various metals in assorted propellant combinations. The results are presented in Table 2.

Although both rhodium and platinum exhibited excellent corrosion-erosion resistance it was decided to use platinum in the needle and the future annular slit configurations, because of its availability and good working characteristics. Rhodium is very brittle and micro cracks tend to form easily. No extensive

Table 2

Summary of Electrochemical Erosion Tests

Anode	Cathode	Electrolyte	Conditions	Results
Gold plated – 20 CB S.S.	Platinum	2 ml H_2SO_4 – 250 ml glycerol (A)	20 volts DC for 3 hours	Black deposit collected on gold but washed off easily. No apparent erosion.
Gold plated – 20 CB S.S.	Platinum	20 gm NaI – 100 ml glycerol (B)	20 volts DC for 1 hour	Heavy deposit of iodine on gold. Considerable erosion.
Gold plated – 20 CB S.S.	Platinum	2.3 gm NaOH – 100 ml glycerol (C)	20 volts DC for 1 hour	Black deposit collected on gold but washed off easily. No apparent erosion.
Rhodium plated brass 100 μ-inch plate 200 μ-inch plate 500 μ-inch plate	Platinum	(B)	20 volts DC for 3 hours	No apparent erosion under 750 × magnification.
Rhodium plated brass 100 μ-inch plate 200 μ-inch plate 500 μ-inch plate	Platinum	(A)	20 volts DC for 3 hours	No apparent erosion under 750 × magnification.
Rhodium plated brass 100 μ-inch plate 200 μ-inch plate 500 μ-inch plate	Platinum	(C)	20 volts DC for 3 hours	No apparent erosion under 750 × magnification.
Platinum plated – 20 CB S.S. – 100 μ-inch plate	Platinum	(A)	Approx. 20 VDC	No apparent erosion.
Platinum plated – 20 CB S.S. – 100 μ-inch plate	Platinum	(C)	Approx. 20 VDC	No apparent erosion.
Platinum plated – 20 CB S.S. – 100 μ-inch plate	Platinum	(B)	Approx. 20 VDC	Iodine collected on platinum but washed off easily – no apparent erosion.

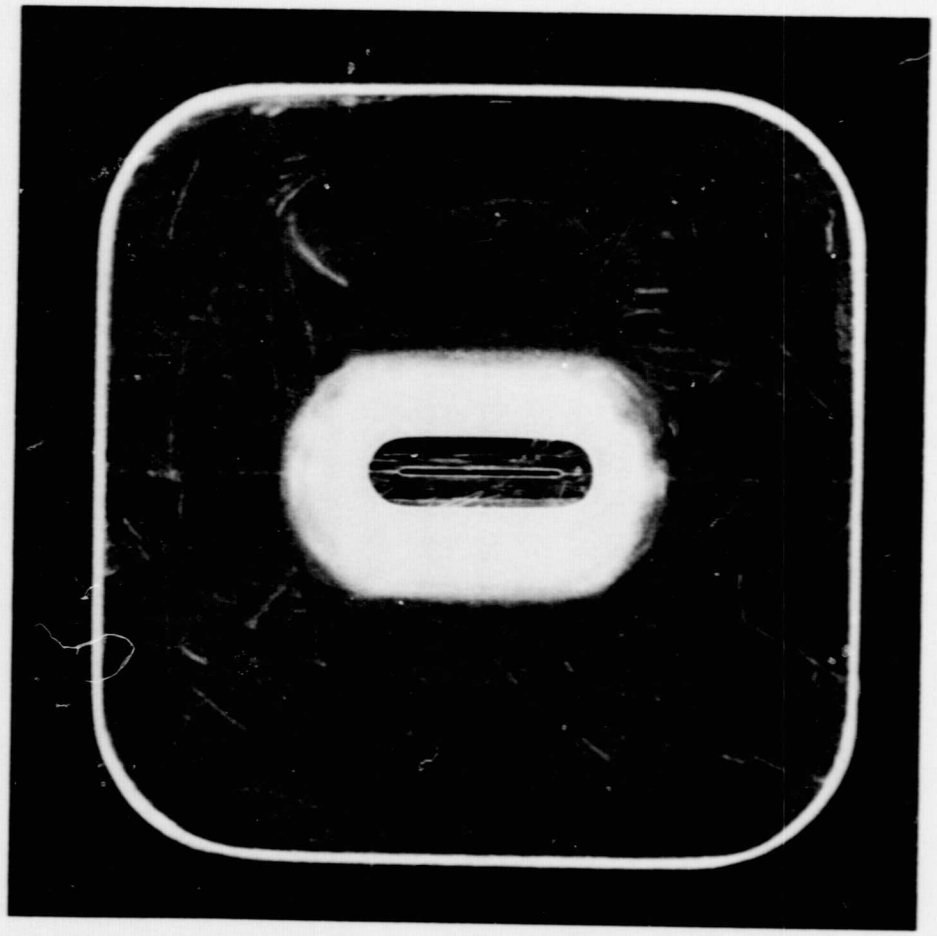

(a) Linear slit thruster.

(b) Annular slit thruster.

Figure 18. Slit configurations.

tests were run on stainless steels, Hastelloy, 20 CB or other similar metals because p(lodic electrochemical tests on these (using them as anodes with a platinum cathode) showed very rapid erosion.

ANNULAR SLIT DESIGN AND PRELIMINARY TESTS

Early in this program considerable throught was given to the various types of configurations that could be used to obtain the high thrust and performance desired.

It is appropriate to state at this time the reasons and advantages for attempting to develop a single high thrust unit rather than depend on the present multiple needle arrays. Assuming that it is possible to get 3 micropounds of thrust per needle it would require more than 30 needles to get 100 micropounds. To get higher thrusts one would require a correspondingly greater number of needles. Considering the fact that these needles must somehow be permanently attached to a common feed system, each surrounded by an extractor and equidistant from each other, presents some technological problems and difficulties. If one needle became damaged it would be extremely difficult to replace it without disturbing or damaging the surrounding needles. Extreme care must be exercised in the handling of such a unit to prevent accidental damage.

A single flow area thruster (e.g. the annular slit) capable of producing the required thrust and overall performance has the obvious advantages of simplicity and convenience. If the rims should become damaged, they can be repolished easily. A linear and an annular slit thruster were consequently designed and built. These are shown in Figures 18a and 18b.

The annular slit was chosen as the configuration to be tested at the conclusion of the needle tests, because its basic slit geometry provides for uniform and uninterrupted electric field intensity lines. This inherently should provide a more uniform spray pattern and hence better general performance characteristics. The following are the basic requirements around which the annular slit design[9] is based.

$$T = 150 \times 10^{-6} \text{ lb}$$

$$I_{sp} = 900 \text{ sec.}$$

$$q/m = 3000 \text{ coulomb/kilogram}$$

$$\dot{m} = \frac{T}{I_{sp}} = \frac{150 \times 10^{-6}}{900} = 1.67 \times 10^{-7} \frac{lb}{sec}$$

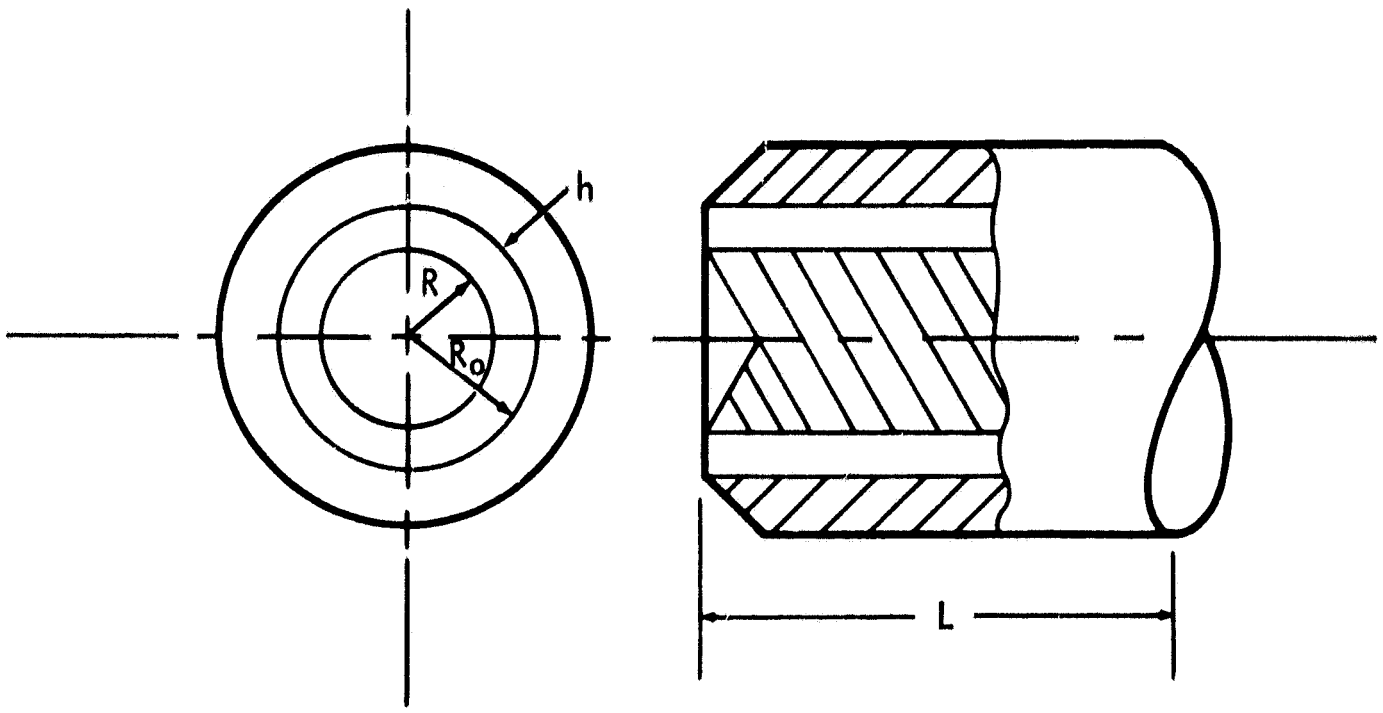

This design was based on the practicality of the smallest machineable dimensions for R and h (slit width). R was chosen as .0400 inches.

Calculations based on the required $\dot{m}$ resulted in

$R_0 = .0422$ inches

$\frac{\Delta P}{L} = 2$

For L = 1.5 inches

$\Delta P = 3$ psi

After the annular slit was fabricated its outer and inner surfaces were plated with 100×10^{-6} inches of platinum. Under this were base platings of nickel and gold amounting to about 70×10^{-6} inches. Before testing the thruster, the rims were polished to about a .0001 inch rim thickness.

There was no problem with polishing the inner rim, however, when the outer rim was polished it was found that hollow bubbles of platinum were coating it, Figure 19. As polishing proceeded these bubbles came off exposing the base metal (20 CB), Figure 20.

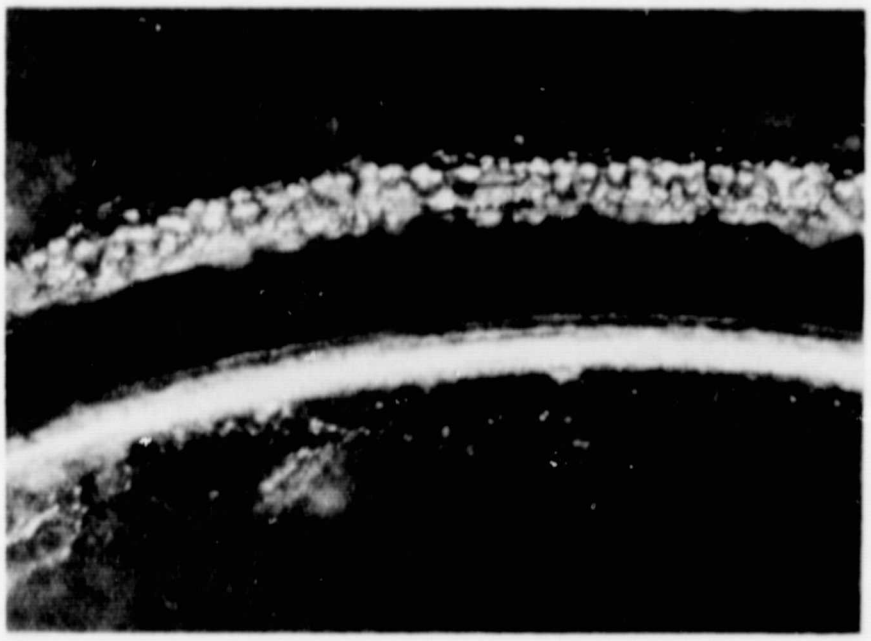

Figure 19. Outer rim platinum plating.

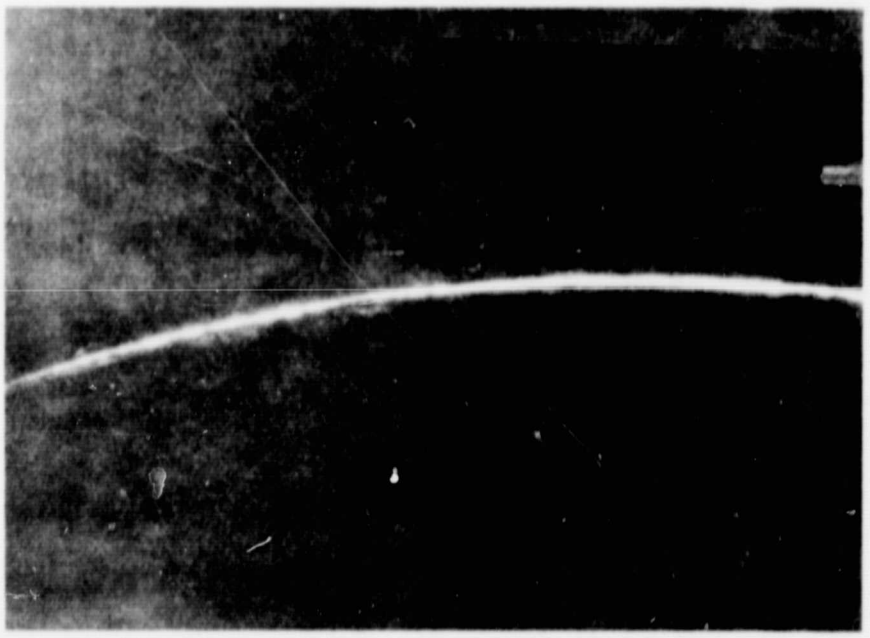

Figure 20. Outer rim after polishing.

The Plating Section at GSFC was consulted as to why this discrepancy existed in plating characteristics between the outer and inner rims. Their explanation was that a "thief" was used around the inner rim surface thus reducing the current density and the rate of platinum plating. However, on the outer rim no "thief" was used and as a result a large current density was present which allowed too rapid a rate of platinum and base metal plating.

With this thruster, preliminary tests were run with a NaI - glycerol propellant solution to prove operational feasibility. Results were very encouraging although the thrust and flow were below design values. Table 3 presents a summary of these initial tests.

FUTURE PROGRAMS

Having proven feasibility of the annular slit thruster, further efforts in this area will be directed towards improving general overall performance so as to more closely approach initial design goals.

The programs as discussed in this section are those considered necessary in order to improve performance.

A. Vertical Mounting

It was decided for future testing to mount the thruster vertically rather than horizontally, as in the initial tests, because during these tests it was observed that propellant spray collected on the bottom segment of the glass vacuum "T" section. No propellant deposit of this order was noted in the top section of the glass "T". The vertical mounting would eliminate the gravity effect on the meniscus since its plane would be parallel to the horizontal. In the horizontal position gravity could cause the meniscus to collect at the bottom giving a poor velocity distribution to the beam.

B. Optimization of Present Configuration

Testing will be directed towards optimizing the extractor configuration and its location with respect to the firing surface. In conjunction with this, tests will be conducted to reduce beam divergence through the use of focusing devices.

C. Sputter Plated Thruster

Presently, a thruster configuration, identical to the one being discussed here, is having its rims plated with platinum by an R-F sputtering technique. This method is supposed to have the advantage of being able to plate a very thin layer of platinum on extremely sharp radii without causing the usual electrochemical problems of excessively thick and nonuniform edges. In fact, it's claimed that the radii plated in such a manner will be sharper than before plating.

If this, in fact, results it may be possible to get good performance parameters at considerably lower thruster voltages.

Table 3

Summary of Initial Tests on Annular Slit

Test No.	Propellent	P_f MM Hg	V_S (KV)	V_{EXT} (Volts)	V_{SCR} (Volts)	I_0 (μa)	I_S (μa)	I_{EXT} (μa)	ACMR	q/m	$\left(\frac{m}{\frac{lb}{sec}}\right) \times 10^{-8}$	$\frac{I_S}{I_0} m \times 10^{-8}$	T (μlb)	$\frac{I_S}{I_0} T$ (μlb)	I_{SP} (sec)	η_b (%)
A.S. 3-2	20 gr NaI 150 ml gly.	128	20	-473	-45	12.8	150	12	2620	1700	1.07	12.5	9.0	105.5	840	64.9
A.S. 8-1	35 gr NaI 117 ml gly.	55	20	-473	-45	13.1	175	4	5079	2852	.569	7.6	6.2	83	1085	56.1
A.S. 9	35 gr NaI 117 ml gly.	113	20.5	-473	-45	13.3	163	6	4813	2643	.609	7.45	6.36	78	1045	54.

D. Propellant Optimization

During the extensive testing of needles and the initial testing of the annular slit thruster wide performance variations were noted between the use of NaI and acids as the dopant in glycerol. Although NaI contributed to a more stable performing propellant the acids produced a more active propellant. This activity of the acids contributed to erratic collector currents with very high peak currents.

It is possible that a three component propellant (e.g., NaI, $H_2 SO_4$ and glycerol) in the right proportions would yield stable performance with higher collector currents.

Of course there are many possible combinations with varying proportions of each component. In addition, an attempt could be made to obtain a different base component which would have greater viscosity stability with temperature variations than glycerol.

This particular investigation, with the great number of combinations possible, would in itself constitute a very time consuming program.

CONCLUSIONS

The needle testing program was varied enough in its scope and depth that a complete familiarization with the technology of electrostatic spraying was possible. With the many tests conducted an understanding was developed of the behavioral characteristics of secondary electron emission inside the vacuum chamber. In addition material erosion characteristics were studied. The ability to test several propellant combinations with varying concentrations created a greater understanding of propellant performance characteristics and their affects on needle material. The testing of various needle tip geometries provided data on affects of rim radius and shape on performance.

With this information and experience it was possible to proceed into the annular slit program with a basic understanding of the principle of electrostatic propulsion and the ability to make sound engineering judgments in testing and design areas. It was possible to plan areas of future research and development required to optimize the annular slit thruster design.

ACKNOWLEDGMENT

The authors wish to express their appreciation to Mr. William Burton who so ably set up and ran the colloid laboratory test facility and was instrumental in

arriving at design concepts, solving testing problems and innumerable other valuable contributions to the overall program.

REFERENCES

1. Beynon, J., et al., Present Status of Colloid Microthruster Technology, AIAA paper 67-531, 1967.

2. Burson, W., Research on Electrohydrodynamic Charged Droplet Beams, AFAPL-TR-67-109, Air Force Aero Propulsion Laboratory, Wright-Patterson Air Force Base, Ohio, October, 1967.

3. Cohen, E., Research on Charged Colloid Generation, APL'TDR 64-75, Air Force Aero Propulsion Laboratory, Wright-Patterson Air Force Base, Ohio, June, 1964.

4. Cohen, E., Experimental Research to Determine the Feasibility of a Colloid Thruster, AFAPL-TR-65-72, 1965.

5. Perel, J., Electrodeless Particle Thruster, AFAPL-TR-67-106, Air Force Aero Propulsion Laboratory, Wright-Patterson Air Force Base, Ohio, October, 1965.

6. Pfeifer, R., Parametric Studies of Electrohydrodynamic Spraying, Report No. CPRL-4-65, Engineering Experiment Station, University of Illinois, 1965.

7. Sherman, A., Parametric Analysis of Electrostatic Dispersion of a Liquid, NASA GSFC X-734-67-321, 1967.

8. Wineland, S., Burson, W., and Hunter, R. E., The Electrohydrodynamic Generation of Charged Droplet Beams, AFAPL-TR-66-72, Air Force Aero Propulsion Laboratory, Wright-Patterson Air Force Base, Ohio, August, 1966.

9. Schlichting, Boundary Layer Theory, McGraw Hill, 1955.

LIST OF SYMBOLS

m = mass flow as measured at the collector

g_0 = acceleration of gravity

v = velocity

T = thrust as measured at the collector

I_{sp} = specific impulse

q/m = SMR charge to mass ratio

I_c = collector current

I = needle or slit currents (use N or S subscript)

η_b = beam efficiency

V = needle or slit voltage (use N or S subscript)

V_{ext} = extractor voltage

P_f = feed pressure

P_t = thruster power

d = time of flight distance

I_0 = TOF collector current at time = 0

t_f = TOF time at current = 0

I_{ext} = extractor current

I_{scr} = screen current (if used)

ACMR = average charge to mass ratio

$\frac{I_N}{I_C} T$ = total thrust

$\frac{I_N}{I_C} m$ = total mass flow